# The role of cyclonic structures in the detachment and separation of Loop Current eddies

- Marco Larrañaga<sup>1,2</sup>, Julien Jouanno<sup>2</sup>, Eric P. Chassignet<sup>1</sup>, Giovanni Durante<sup>4</sup>,

  Ilkyeong Ma<sup>1</sup>, Julio Sheinbaum<sup>4</sup>, Lionel Renault<sup>2</sup>
- <sup>1</sup>Center for Ocean-Atmospheric Prediction Studies (COAPS), Florida State University, Florida, USA
- <sup>2</sup>LEGOS, Université de Toulouse, CNES-CNRS-IRD-UPS, 14 Avenue Edouard Belin, 31400 Toulouse,
- France.
- <sup>4</sup>Center for Scientific Research and Higher Education at Ensenada (CICESE), Ensenada, Mexico.

## Key Points:

10

13

- An altimetry-based and latitude-dependant analysis of the Loop Current eddy shedding process
  - The merging of cyclonic eddies from both sides of the LC is essential for the separation process
  - Latitude of separation has consequences on the properties of the LCEs

Corresponding author: Marco Larrañaga, marco.larranaga@fsu.edu

#### Abstract

15

16

17

18

19

20

21

22

24

25

26

27

29

30

31

32

33

34

35

36

37

39

40

41

42

43

44

45

46

47

The Loop Current (LC) and its associated eddies, known as Loop Current Eddies (LCEs), are key oceanic features in the Gulf of Mexico. Analysis of 29 years of satellite altimeter data (1993-2021) shows that more than half of the LCEs that detach from the LC reattach within 30 days and that only 42% truly separate from the LC and move westward in the Gulf. We find that i) before a detachment can occur, the LC needs to extend far enough north in the Gulf to reach the Mississippi fan ( $\sim 27.5^{\circ}$ ); ii) the ratio of separations to reattachments depend on latitude, with detachments being more prone to reattach if they occur south of 25°N and to separate if they occur north of 25°N; and iii) cyclonic eddies are always present during the detachment process, with one cyclonic eddy on the eastern side of the LC if the LCE is to reattach and one cyclonic eddy on each side of the LC is the LCE is to separate. In the latter case, the co-occurrence of eastern and western cyclonic eddies in the LC bottleneck zone forms a large cyclonic structure. This structure may hinder the reattachment of newly formed LCEs and, therefore, modulate the extension of the LC into the Gulf of Mexico. Sometimes, it can restrict LC growth on time scales of several months. The results highlight the pivotal role that cyclonic eddies play in detachment events.

#### Plain Language Summary

Loop Current Eddies (LCEs) are large anticyclonic structures in the Gulf of Mexico that frequently detach from the Loop Current. These eddies play an important role in modulating the ocean dynamics of the Gulf and influencing economic activities, such as offshore oil and gas extraction. Predicting LCE separation events and their subsequent trajectories is crucial. To achieve this, it is essential to understand both the conditions driving LCE detachment and those that prevent the Loop Current from reattaching the eddies. This study demonstrates that the latitude of detachment, along with the presence of energetic cyclonic eddies on both sides of the detachment zone, are key factors influencing the final separation of LCEs

## 1 Introduction

The Gulf of Mexico (GoM) is a semi-enclosed basin, with dynamics dominated by the Loop Current (LC), an anticyclonic current that originates in the Yucatan Channel and extends into the Florida Straits. Episodically, the LC sheds anticyclonic warm-core rings, known as Loop Current Eddies (LCEs), with diameters larger than 200 km (Biggs et al., 1996; Leben, 2005). Once an LCE detaches, it may reattach multiple times

to the LC or separate definitively, traveling westward across the GoM. The periodicity of these separation events is highly variable, ranging from 100 to 400 days (Leben, 2005; Dukhovskoy et al., 2015; Garcia-Jove et al., 2016; Larrañaga et al., 2022). LCEs play a crucial role in the oceanic and atmospheric dynamics of the GoM. As they move west-ward, they transport warm water from the Caribbean Sea into the GoM (Bunge et al., 2002; Sosa-Gutiérrez et al., 2020; Hamilton et al., 2018; Meunier et al., 2018, 2020) and can contribute to the rapid intensification of hurricanes by serving as a heat reservoir (Molina et al., 2016; Yablonsky & Ginis, 2012). Moreover, LCEs have economic implications, particularly by disrupting oil and gas production from unanchored platforms (Kantha, 2014). 

The mechanisms behind the detachment and separation of LCEs are not yet fully understood. Hurlburt and Thompson (1980) highlighted the importance of differential rotation, suggesting that the Earth's differential rotation ( $\beta > 0$ ) is essential for realistic eddy shedding. This was later confirmed by Pichevin and Nof (1997), who linked LCE detachment to the propagation of a long Rossby wave that outpaces LC growth. However, this theory assumes that the LC returns to its initial position after detachments, which is not always observed in reality (Leben, 2005). Leben (2005) and Lugo-Fernández and Leben (2010) showed that the retreat latitude of the LC after separations is inversely correlated with the time between separations, with separation periods longer than 10 months when the LC retreats below 25°N, and around 5 months when it retreats above this latitude.

Chérubin et al. (2006) used a numerical approach to indicate that LCE detachment results from a combination of baroclinic energy conversion in the deep GoM layers and barotropic energy conversion in the upper layers. Donohue et al. (2016) and Hamilton et al. (2016) analyzed three LCE separations using a mooring array located between the Campeche Bank, the Mississippi Fan, and the West Florida Shelf. Their findings indicated that LCE detachments are associated with an increase in deep EKE, coinciding with large-scale meanders in the northern and eastern LC regions. They concluded that this increase in EKE results from the conversion of available potential energy to EKE. Conversely, Yang et al. (2023) found that barotropic energy conversions dominated the energy balance during detachment events.

Cyclonic eddies are omnipresent in the Gulf and it has been suggested that they play a critical role in the LCE shedding process (Cochrane, 1972; Vukovich & Maul, 1985; Fratantoni et al., 1998; Chérubin et al., 2006; Le Hénaff et al., 2012; Nickerson et al., 2022). Three main types of cyclonic eddies in the Gulf have been identified: cyclonic eddies that originate in the Caribbean Sea (Candela et al., 2002; Athié et al., 2012; Jouanno et al.,

2016); frontal eddies generated east of the Campeche Bank, which travel along the LC (Jouanno et al., 2016; Hiron et al., 2020); and persistent cyclonic eddies near the Dry 85 Tortugas, also known as Tortugas eddies (Fratantoni et al., 1998). Several scenarios involving cyclonic eddies in LCE detachment have been proposed. One of them is that de-87 tachment can be triggered by the intensification of eddies on the eastern side of the LC 88 (e.g., Tortugas eddy), via the merging of a train of frontal eddies propagating along the LC (Fratantoni et al., 1998; Le Hénaff et al., 2012). Another widely discussed process 90 involves cyclonic eddies "pinching off" the LC from its eastern and western flanks, effectively cutting the LC transversely (Schmitz, 2005; Fratantoni et al., 1998; Zavala-Hidalgo 92 et al., 2003). Finally, LCE separations have also been shown to correlate with the ar-93 rival of Caribbean eddies into the GoM (Athié et al., 2012; Jouanno et al., 2016; Sheinbaum et al., 2016). This is in agreement with the findings of Le Hénaff et al. (2023), who 95 identified Caribbean eddies as key factors in forecasting LCE separation. However, Garcia-Jove et al. (2016) point out that although Caribbean Cyclonic eddies can modulate the 97 occurrence of LCE separations, they are not essential for their occurrence, reflecting on-98 going debate on the overall role of Caribbean Cyclonic eddies in the shedding process.

In this paper, we systematically document the role of cyclonic structures in the detachment and separation of LCEs by analyzing 29 years of satellite altimeter data (1993-2021). We show that cyclonic eddies are always present during the detachment process, with one cyclonic eddy on the eastern side of the LC if the LCE is to reattach, and one cyclonic eddy on each side of the LC if the LCE is to separate. In the latter case, the co-occurrence of eastern and western cyclonic eddies in the LC bottleneck zone forms a large cyclonic structure. This structure may hinder the reattachment of newly formed LCEs and modulate the extension of the LC into the Gulf of Mexico. Sometimes, it can restrict LC growth on time scales of a few months. The paper is organized as follows: Section 2 outlines the data and methods. The following sections examine the key mechanisms driving LCE detachment and separation, as well as the role of cyclonic eddies in these processes. Results are summarized and discussed in Section 6.

#### 2 Data and methods

100

101

102

103

104

105

106

107

108

109

110

111

112

113

114

115

116

117

118

This study analyzes 29 years of altimetry gridded data from 1993 to 2021, provided by CMEMS (European Union-Copernicus Marine Service, 2015), accessed on October 15, 2024. Daily maps of Absolute Dynamic Topography (ADT) with a 1/4° horizontal resolution are created by adding Sea Level Anomaly (SLA) maps to the MDT-CNES-CLS22 mean dynamic topography product from AVISO (Jousset et al., 2025). Following Leben (2005), the LC and LCE fronts are tracked using the 17-cm contour in demeaned

SSH fields. Removing the basin-scale mean is necessary to eliminate a bias associated with seasonal height variations due to warming and cooling of the upper ocean (Dukhovskoy et al., 2015). Demeaned fields are calculated by subtracting the spatial mean over the area defined by the longitudes 99 to 80°W and latitudes 17 to 31°N from each daily SSH field.

Other methods exist for detecting the position of the LC, such as the approach by Laxenaire et al. (2023), which identifies the LC using a contour associated with the maximum geostrophic velocity magnitude between the Yucatan Channel and the Florida Straits. However, Laxenaire et al. (2023) showed that both methods yield similar results.

Detachment events are identified by visually inspecting the daily ADT fields and as taking place when the 17-cm contour splits into two distinct loops: one corresponding to the LC and the other to the detached LCE. A detachment event is classified as a separation if the newly formed LCE does not reattach to the LC and travels westward across the GoM. Each reattachment is treated as an independent event, regardless of whether the same LCE reattaches multiple times before its final separation. To latitudinally classify detachment, reattachments, and separation events, we compute the outermost position of the LC following a detachment. This position corresponds to the spatial coordinate of the LC that is closest to the periphery of a detached LCE. This reference point allows us to distinguish between events occurring at different latitudes.

Additional datasets are used to complement the ADT satellite measurements, including current-meter observations along the Yucatan Channel and an atlas of eddy trajectories over the GoM and Caribbean Sea. The current-meter data were obtained from a mooring array deployed by the CANEK research group at CICESE (Ensenada Center for Scientific Research and Higher Education) in the Yucatan Channel, covering the period from July 2012 to October 2020 (Sheinbaum, 2002; Durante et al., 2023; Candela et al., 2019). The Mesoscale Eddy Trajectory Atlas 3.2 (META) (Pegliasco et al., 2022) delayed-time product is from AVISO, which uses an eddy detection method based on Chelton et al. (2011) to identify and track the eddies from the CMEMS Daily ADT maps.

# 3 29 years of LC detachment, reattachment, and separation statistics

We begin by documenting the detachment statistics of LCEs from 29 years of altimetry data (Figures 1 and 2). We classify them into those that reattach to the Loop Current (hereafter referred to as reattachment events) and those that completely separate and move westward in the Gulf of Mexico (hereafter referred to as separation events). Details of each detached eddy, including the date, region, and eddy name, are provided

in Tables S1 and S2 in the Supporting Information. In total, 92 detachment events were identified between 1993 and 2021. Of these, 53 eddies (58%) reattached to the Loop Current, while 39 (42%) fully separated and drifted westward into the Gulf of Mexico. These detachment statistics highlight that reattachments are relatively common (3 per year on average) and deserve to be more closely examined, given their potential role in modulating LC dynamics and eddy shedding statistics.

The detachment statistics also show that the detachment locations, defined by the outermost position of the Loop Current following each detachment, span a broad latitudinal range, from 22°N to 28°N (Figure 1a). These events can be grouped into three distinct latitudinal clusters:

- Detachments above 26°N: This group includes 10 detachment events characterized by a wide zonal spread, extending from 90°W to 86°W.
- Detachments between 24°N to 26 °N: Comprising 50 detachment events, this is
  the most densely populated cluster. It exhibits a narrow horizontal extent, constrained between the Campeche Bank and the West Florida Shelf.
- Detachments below 24°N: This cluster includes 28 events, most of which are skewed toward the Campeche Bank.

Additional insights are gained by separating the detachment locations from events when LCEs reattach to the LC (Figure 1b) from those that fully separate and drift westward (Figure 1c). Detachments that lead to reattachment events are predominantly concentrated south of 25°N, accounting for 75% of such cases. In contrast, separation events display greater spatial variability in their detachment positions. There are notable differences in the mean position of the LC one day prior to detachment (defined as the 17-cm contour extracted from the ADT field averaged across all detachments, reattachments only, and separations only, respectively - Figures 1b-c). For reattachments, the LC typically displays a well-defined bulb-like structure with a pronounced eastern bottleneck, and the detachment locations are tightly grouped together west of this bottleneck. Conversely, in the separation cases, the detachment locations are more spread out latitudinally and the average LC shape is more elongated and exhibits standing meanders on both sides of the LC.

From Figures 1 and 2, we can make the following statements:

1. Detachments occurring south of 25°N are more prone to reattach (73%) while those occurring north of 25°N are more prone to separate (64%),

- 2. A minimum length of ~1800 km for the LC is required before a detachment can occur (Figure 2a). This distance corresponds to the LC reaching the Mississippi Fan, a Gulf shelf slope situated southeast of the Mississippi Delta (Figure 1a). The probability density function (in color in Figure 1), representing the spatial occurrence of the LC prior to the detachments, shows that between 60 and 70% of detachment, reattachment, and separation events occur when the LC is close to this bathymetric feature.
  - South of 26°N, the length of the LC has no influence on the latitude at which detachments occur.
- 4. Detached LCEs are much larger when detachments occur in the southern part of the domain (Figure 2b), with eddies exceeding 300 km in diameter when detached south of 24°N, compared to around 150 km when detachment locations occur north of 26°N. This is not too surprising since the LC is limited in its northward extent.
- 5. There is no obvious relationship between the kinetic energy of the LCEs (Figure 2c) and the detachment latitude. The most energetic LCEs (about  $0.2 \text{ m}^2 \text{ s}^{-2}$ ) occur between  $24\text{-}25^{\circ}\text{N}$ .

In the following sections, we quantify the role that cyclonic eddies play in LCE detachments as a function of latitude and investigate the origin of the western cyclonic structures leading to separation events.

## 4 On the role of cyclonic eddies in LC detachments

Quantification of the dynamical differences between separation and reattachment cases can be obtained by analyzing composite SLA and relative vorticity  $(\zeta/f)$  fields at the time of detachment (Figure 3). To illustrate the latitudinal dependence and different dynamics, we refine our previous classification by grouping detachment, separation, and reattachment over: i) latitudes below 24°N, ii) latitudes between 24 and 25°N, iii) latitudes between 25 and 26°N, iv) latitudes above 26°N with detachments west, and v) latitudes above 26°N with detachments east of the Mississippi Fan.

The composites show that LCE detachments occurring south of 26°N, regardless of whether they separate or reattach, all involve negative SLA structures on the eastern side of the LC (Figures 3a<sub>1</sub>-a<sub>3</sub>, and 3b<sub>1</sub>-b<sub>3</sub>). Unlike reattachment cases (Figures 3a<sub>1</sub>-a<sub>3</sub>), separations are also characterized by the presence of negative SLA structures to the west of the LC (Figures 3b<sub>1</sub>-b<sub>3</sub>). The relative vorticity composites of detachment events show that these negative SLA structures are associated with closed cyclonic circulation, suggesting the presence of mesoscale cyclonic features during the detachment of LCEs

221

223

224

225

226

228

229

230

231

232

233

234

235

236

237

238

239

240

241

242

243

244

245

246

247

249

250

251

252

253

254

255

(Figures 3c<sub>1</sub>-c<sub>3</sub>, and 3d<sub>1</sub>-d<sub>3</sub>). The latter is confirmed by independently computing the histogram of cyclonic eddy occurrences using the AVISO Mesoscale Eddy Trajectory Atlas 3.2 (META), which shows that cyclonic eddies are present in more than 70% of detachment events (Figures 3e<sub>1</sub>-e<sub>3</sub> and 3f<sub>1</sub>-d<sub>3</sub>). Unlike detachments south of 26°, the SLA and relative vorticity composites of separation events north of 26°N, both west and east of the Mississippi Fan, show only a weak signal of cyclonic circulation northwest and southwest of the LC at the time of detachment (Figures 3b<sub>4</sub>-b<sub>5</sub>,d<sub>4</sub>-d<sub>5</sub>,f<sub>4</sub>-f<sub>5</sub>). North of 26°N, reattachment events are rare (only 2 events east of the Mississippi Fan over a 29-year period (Figure 3a<sub>4</sub>-a<sub>5</sub>,c<sub>4</sub>-c<sub>5</sub>,e<sub>4</sub>-e<sub>5</sub>), making it difficult to differentiate between conditions that are conducive to reattachment or separation.

In order to investigate in more detail the relationship between the separation of LCEs and the presence of cyclonic eddies, we compare time-evolution composites of reattachment and separation events from 45 days before to 30 days after detachment (Figures 4, 5, 6,7, 8). This time window was chosen since 80% of the detached eddies are reabsorbed by the LC within 30 days (Figure S1). South of 26°N, in the days leading up to a detachment, whether it results in reattachment or separation, cyclonic eddies east of the Florida Shelf grow in size and contribute to a narrowing of the LC neck (first three columns in Figures 4, 5, 6, and 9). This pattern suggests that the intensification of a cyclonic eddy between the LC and the Florida Shelf contributes to eddy shedding events. This intensification has been linked to the merging of frontal eddies by Le Hénaff et al. (2012). In addition, during separation events, there is a second cyclonic eddy west of the LC that is present in all cases and is strongest around the time of detachment (fourth column in Figures 4, 5, 6). This eddy appears  $\sim 15$  days before separation in the 24-25°N cases (Figure 5) and earlier in the 25-26°N cases (from -30 to -15 days; Figure 6). The development of these western cyclonic eddies alters the shape of the LC during eddy detachment and contributes to the final separation by effectively "pinching off" the LC from both sides (Schmitz, 2005). Specifically, cyclonic eddies west of the LC tend to shift the LC away from the Campeche Bank, a configuration not observed during reattachment events (Figures 4, 5, 6 and third row in Figure 9).

There is a difference in the separation processes that occur south of 25°N and between 24-25°N that we believe can be largely attributed to the position of the cyclonic eddies east and west of the LC. In the separations that take place south of 25°N, the eastern cyclonic eddy is located southeast of the LC near the Dry Tortugas (third and fourth columns in Figure 5) and is often referred to as a Tortugas Eddy (Fratantoni et al., 1998). By contrast, during the 25-26°N separations, the cyclonic eddy is located northeast of the LC (third and fourth columns in Figure 6). The time-evolution composites indicate

that the development of this northeast cyclonic eddy tends to emerge when no Tortugas eddies are present east of the LC at the time when a western cyclonic eddy appears. When a Tortugas eddy is present, as in the south of 25°N cases, the occurrence of a western cyclonic structure will promote the separation of a LCE via the "pinch off" mechanism (third and fourth rows in Figure 5). In the absence of a Tortugas eddy, the western cyclonic eddy will cause the LC to move east toward the Florida Strait, obstructing the passage of trailing cyclonic eddies and favoring their merging at this northeastern location (second to fifth rows in Figure 6). The merging of frontal eddies northeast of the LC has been documented by several authors, including Zavala-Hidalgo et al. (2003), Le Hénaff et al. (2012), and Hiron et al. (2020).

For separations occurring above 26°N, they occur mostly east or west of the Mississippi Fan (Figure 1c) and we therefore make a geographical distinction when making the composites. In all cases, during the 45 days leading up to detachment, cyclonic eddies are observed to migrate northward between the Campeche Bank and the western edge of the LC at the same time that cyclonic eddies are present northwest of the Florida Shelf (first three columns in Figures 7 and 8). For separation events occurring east of the Mississippi Fan, composites show a recurring intensification of cyclonic eddies northwest of the Florida Shelf, which promote detachment and reattachment events during the 30 days preceding the final detachment (first three columns in Figure 7). During this time period, cyclonic eddies on both sides of the LC merge into a large cyclonic eddy west of the LC, near 25°N (second and third columns in Figure 7). Final detachment of LCEs occurs when the cyclonic eddies "pinch off" the LC from both sides. The process is very similar for separations occurring west of the Mississippi Fan, but the main difference is that once an LCE is formed, it never reattaches (Figure 8). Reattachments can occur when the LCE is formed east of the Mississippi Fan since the separation point is east of the main axis of the LC (Figure 1c).

The above results highlight the role of cyclonic eddies in promoting the detachment of LCEs. In order to get insights as to why LCEs detached by a single cyclonic eddy east of the LC are more likely to reattach south of 26°N, while those detached by cyclonic eddies on both sides of the LC are more likely to separate, we now analyze composites up to 30 days following a detachment (fifth and sixth columns in Figures 4,5, 6, and 9).

In the days after a separation (final detachment), all lagged composites at days 15 and 30 show the presence of large cyclonic features acting as barriers between the LC and LCEs (fifth and sixth rows in Figures 4, 5, and 6). These large cyclonic features typically result from the merging of cyclonic eddies originating from both sides of the LC neck, and their presence appear to prevent the LC from reattaching to the detached ed-

dies. These cyclonic structures (hereafter referred to as barrier eddies) have been documented in several observational studies. For instance, Zavala-Hidalgo et al. (2003) and Zavala-Hidalgo et al. (2006) showed that they can last up to nine months and that they may play a significant role in inhibiting the LC penetration into the GoM for several months. By contrast, when there is only one cyclonic eddy east of the LC at the time of detachment, it is not strong enough to prevent the LCE from reattaching to the LC (fifth and sixth columns of Figure 9).

To further illustrate the impact of barrier eddies on the LC northward penetration after separation, we analyze their persistence by generating a histogram of their spatial distribution and persistence in time between separation events (Figure 10a-c). On average, the barrier eddies persist for more than four months northwest of the LC after separations that occurred below 24°N, three months after separations between 24 and 25°N, and one month after separations between 25 and 26° (Figure 10a-d). Furthermore, the LC does not penetrate into the GoM four months (thin dashed line) after separation events below 24°N, three months (thin black line) after separations between 24 and 25°N, and one month (thick black line) after separation between 25 and 26°N (Figure 10a-c). This suggests that the further south the detachment occurs, the longer the barrier eddy tends to persist, possibly preventing a LC extension into the GoM. For separations north of 26°N, the barrier eddy does not last and does not have any impact on the LC evolution. This barrier eddies may help explain why, as noted in Leben (2005) and Lugo-Fernández and Leben (2010), southern separations are typically followed by longer separation periods.

#### 5 The origin of western cyclonic structures leading to separations events

From the analysis above, cyclonic eddies on the west side of LC play an essential role in the final detachment of an LCE and the question then arises as to their origin. Are they formed locally, or are they advected from the Caribbean Sea? Composite Hovmöller diagrams of SLA and the spatial occurrence of cyclonic eddies from the Mesoscale Eddy AVISO Atlas (Pegliasco et al., 2022) were constructed following transects that extend from the Caribbean and Yucatan coasts, crossing the LC at the respective detachment locations, and spanning from 120 days before to 30 days after each detachment (Figure 11). The transects are shown in the fourth column of Figures 4, 5, 6, 7, and 8. For the separations south of 26°N, the diagrams show the presence of negative SLA anomalies propagating from latitudes as far south as the Chinchoro Bank (e.g., diamond marker in the fourth column of Figure 1). In each case, these anomalies intensify as they cross the Yucatan Channel, giving rise to cyclonic structures west of the LC. These western

328

330

331

332

333

335

336

337

338

339

340

341

342

343

344

345

346

347

348

349

350

351

352

353

354

355

356

357

359

360

361

362

cyclonic features can be seen to merge with the cyclonic structures that are located to the north or east of the LC, giving rise to the barrier eddies described in the previous section. There is a striking difference in the path of the negative SLAs as a function of latitude. For southern separations, the cyclonic features can be detected as far south in the middle of the Caribbean Sea, while for northern separations, they are generated locally in the GoM, north of the Yucatan Channel (see negative SLA trajectories in Figure 11). Furthermore, there is a huge contrast between the Hovmöller SAL diagrams for separations (Figure 11) and reattachments (Figure 12). The signature associated with negative SLAs propagating from the Caribbean, seen in Figure 11 for separations, is completely absent in Figure 12 for reattachments (as surmised from the analyses of the composites).

The above Hovmöller composites clearly show northward propagation of negative SLAs from the Caribbean Sea, but how do we ensure that they are associated with eddies? From the Mesoscale Eddy AVISO Atlas, mesoscale eddies can be detected on the negative SLA propagation prior to the separation, but only in the GoM (right column of Figure 11). There are well-known limitations in the construction of the gridded datasets used to track eddies from altimetry (Chelton et al., 2011; Hogg et al., 2015; Amores et al., 2018; Archer et al., 2020) and the amplitude of mesoscale eddies can be underestimated when interpolating from altimetric tracks to gridded data (Hogg et al., 2015). This is the case for Caribbean eddies, as shown by the comparison of the CMEMS SLA estimations from AVISO with those from the new satellite mission SWOT (Surface Water and Ocean Topography; Morrow et al. (2019)). Negative SLA anomalies associated with Caribbean cyclonic structures are clearly identified in the SWOT data, whereas their amplitude is largely underestimated in the CMEMS data (Figure 13). Although the SWOT mission provides a more accurate representation of the mesoscale eddies, its 120-km swath and 21-day repeat cycle result in insufficient temporal resolution for tracking the propagation of Caribbean cyclonic eddies. Inclusion of the SWOT data in the CMEMS gridded altimetry products is under development and should lead to an improved eddy atlas. While the SWOT data provides anecdotal evidence that strong cyclonic structures are present in the Caribbean Sea and near the Yucatan Channel (Figure 13), they do not demonstrate northward propagation. However, in agreement with Sheinbaum et al. (2016) and Athié et al. (2012), Hovmöller diagrams of SLAs in the Yucatan Channel do show significant east-west displacements associated with separations (see 17 cm contour in Figures 14a-e), which could be signatures of northward propagation of cyclonic features. These displacements are also found by constructing the Hovmöller diagrams of zonal velocities derived from 10 years of current-meter observations from the CANEK program, spanning July 2012 to October 2020 (Sheinbaum, 2002; Athié et al., 2012, 2015;

Sheinbaum et al., 2016; Candela et al., 2019; Athié et al., 2020). Although the number of events captured by the in-situ CANEK observations is limited compared to the altimeter record, the time-evolving composites of the current velocities do show an eastward displacement of the LC (Figure 14f-h) prior to separations with negative velocities west of the main axis of the Yucatan Current, indicative of cyclonic structures. This eastward shift is particularly evident in detachments occurring below 24°N and between 25 and 26°N. In both cases, negative velocities are observed west of the LC, extending down to depths of 300 m (Figure 14k-m).

### 6 Summary and discussion

365

367

368

369

370

371

372

373

374

375

377

378

379

380

382

383

385

386

387

388

390

391

392

393

395

398

399

The mechanisms behind LCE detachment and the fate of the LCEs, including whether they reattach or separate, have been a subject of studies long before altimeter data became available (Elliott, 1982). We now have an unprecedented record of 29 years of altimetry measurements, and its analysis shows that, over that time period, we have 92 LCE detachments, of which 53 (58%) reattach to the LC and 39 (42%) truly separate from the LC. We believe that our analysis demonstrates that cyclonic structures are fundamental for the detachment of LC eddies, by pointing out that an LCE detachment will be more likely not to reattach to the LC when cyclonic structures are present on both sides of the LC and "pinch off" an eddy. The main reason for this final detachment and separation is the formation of a large cyclonic structure, which we define as barrier eddy, that results from the merging of the cyclonic features on both sides of the LC. This barrier eddy physically separates the LC from the freshly separated LCE and allows the latter to move westward. Furthermore, this barrier eddy may hinder the LC penetration into the GoM. Barrier eddies can persist after separation for up to several months northwest of the LC, depending on the separation latitude, longest for southern separations and shortest for northern separations. By contrast, LCE detachments triggered by intensified cyclonic structures occurring only east of the LC are more likely to reattach since there are no barrier eddies to isolate the freshly separated eddy from the LC. A key outcome of our analysis is the classification of detachment events as a function of latitude. This basic clustering highlights important differences in the dynamics of LCE separation depending on the latitude at which detachment occurs. Specifically, we find that i) a minimum length of  $\sim 1800$  km for the LC is required before a detachment can occur. This distance corresponds to the LC reaching the Mississippi Fan, a Gulf shelf slope situated southeast of the Mississippi Delta; ii) South of 26°N, the length of the LC has no influence on the latitude at which detachments occur; and iii) detached LCEs are much larger when detachments occur in the southern part of the domain, with eddies exceeding 300 km in diameter when detached south of 24°N, compared to around 150 km when

detachment locations occur north of 26°N. This is not too surprising since the LC is limited in its northward extent.

400

401

402

403

404

405

406

407

409

410

411

412

413

414

415

416

417

418

419

420

421

422

423

424

425

426

427

428

429

430

431

432

433

434

We assess that cyclonic anomalies propagating from the Caribbean appear to play a key role in the separation process, and there is a striking difference as a function of latitude in the path of the western cyclonic eddies that lead to separation. For southern separations, the cyclonic features can be detected as far south in the middle of the Caribbean Sea, while for northern separations, they are generated locally in the GoM north of the Yucatan Channel. The passage of those cyclonic features can be documented through an eastward displacement of the LC observed in altimetry data and by the occurrence of negative velocities west of the LC in the CANEK mooring array, both coinciding with the passage of cyclonic anomalies through the Yucatan Channel in our Hovmröller composites. There are no cyclonic features propagating north from the Caribbean in reattachments. However, questions remain regarding the nature of the cyclonic features: Are they simply vorticity anomalies associated with the boundary current, or do they represent coherent cyclonic eddies? It is noteworthy that negative SLA signals propagating from the Caribbean to the Gulf of Mexico during separations below 26° are not detected by traditional eddy detection methods, since the amplitude of these features is often underestimated due to the interpolation of altimeter track data into gridded fields (Chelton et al., 2011; Hogg et al., 2015; Amores et al., 2018; Archer et al., 2020). This underestimation is especially pronounced for cyclonic structures in the Caribbean Sea when comparing SLA from gridded altimeter and SWOT observations. However, the comparison between SLA maps and in-situ CANEK measurements suggests that, despite the challenges of detecting cyclonic eddies in this region using standard altimetry products, there is clear evidence that cyclonic structures are being advected within the Yucatan Current. While the SWOT mission provides a more accurate representation of the mesoscale eddies, its 120-km swath and 21-day repeat cycle result in insufficient temporal resolution for tracking the propagation of Caribbean cyclonic eddies. Nevertheless, the combination of altimeter constellations and SWOT could improve the detection of Caribbean cyclonic eddies. Additionally, future satellite missions such as ODYSEA, the Ocean DYnamics and Surface Exchange with the Atmosphere mission (Rodríguez et al., 2019; Wineteer et al., 2020; Torres et al., 2023; Larrañaga et al., 2025), are expected to address these limitations by measuring total sea surface currents with a 5-km resolution, 1700-km swath, and 4-day repeat cycle. This improved spatial and time resolution could enable a more accurate representation of the Caribbean cyclonic eddies and their propagation into the GoM.

Finally, to further document and demonstrate the impact of Caribbean, one could perform process studies in which numerical simulations that explicitly include or exclude Caribbean eddies at the boundaries could help us quantify the relative importance of locally generated cyclonic eddies to eddies coming from outside the GoM in the separation of LCEs. Similarly, one could easily investigate the role of the barrier eddies in modulating the northward extension of the LC by performing numerical experiments with and without a barrier eddy in front of the LC for different LC extensions.

## 7 Data Availability Statement

The daily gridded altimetry data used in this study, including Absolute Dynamic 443 Topography, Sea Level Anomaly, and the MDT-CNES-CLS22 mean dynamic topogra-444 phy, are publicly available from the Copernicus Marine Environment Monitoring Service 445 (CMEMS) at https://marine.copernicus.eu, accessed on October 15, 2024. The Mesoscale 446 Eddy Trajectory Atlas 3.2 (META) delayed-time product, used for eddy trajectory in-447 formation, is available from AVISO at https://www.aviso.altimetry.fr. The current-meter 448 data from the Yucatan Channel were obtained from a mooring array deployed by the CANEK 449 research group at CICESE. These data are available upon reasonable request from Julio Sheinbaum (julios@cicese.mx). 451

## 452 Acknowledgments

435

436

438

439

440

441

442

The PhD grant for ML was supported by CNES and Université Paul Sabatier. The authors appreciate the support from the UGOS program of the National Academies of Science (Grant Number: 200013149).

#### References

456

Amores, A., Jordà, G., Arsouze, T., & Le Sommer, J. (2018). Up to what extent can 457 we characterize ocean eddies using present-day gridded altimetric products? 458 Journal of Geophysical Research: Oceans, 123(10), 7220–7236. 459 Archer, M. R., Li, Z., & Fu, L.-L. (2020, June). Increasing the space-time resolution of mapped sea surface height from altimetry. Journal of Geophysical Research: 461 Oceans, 125(6). Retrieved from https://doi.org/10.1029/2019jc015878 462 doi: 10.1029/2019jc015878 463 Athié, G., Candela, J., Ochoa, J., & Sheinbaum, J. (2012, March). Impact of caribbean cyclones on the detachment of loop current anticyclones. Journal of Geophysical Research: Oceans, 117(C3), n/a-n/a. Retrieved from 466 https://doi.org/10.1029/2011jc007090 doi: 10.1029/2011jc007090

- Athié, G., Sheinbaum, J., Candela, J., Ochoa, J., Pérez-Brunius, P., & RomeroArteaga, A. (2020, February). Seasonal variability of the transport through the
  yucatan channel from observations. Journal of Physical Oceanography, 50(2),
  343–360. Retrieved from https://doi.org/10.1175/jpo-d-18-0269.1 doi:
  10.1175/jpo-d-18-0269.1
- Athié, G., Sheinbaum, J., Leben, R., Ochoa, J., Shannon, M. R., & Candela, J.

  (2015, March). Interannual variability in the yucatan channel flow. Geophys
  ical Research Letters, 42(5), 1496–1503. Retrieved from https://doi.org/
  10.1002/2014g1062674 doi: 10.1002/2014g1062674
- Biggs, D. C., Fargion, G. S., Hamilton, P., & Leben, R. R. (1996, September).

  Cleavage of a gulf of mexico loop current eddy by a deep water cyclone. Journal of Geophysical Research: Oceans, 101(C9), 20629–20641. Retrieved from

  https://doi.org/10.1029/96jc01078 doi: 10.1029/96jc01078
- Bunge, L., Ochoa, J., Badan, A., Candela, J., & Sheinbaum, J. (2002, December).

  Deep flows in the yucatan channel and their relation to changes in the loop

  current extension. Journal of Geophysical Research: Oceans, 107(C12), 26–

  1–26–7. Retrieved from https://doi.org/10.1029/2001jc001256 doi:

  10.1029/2001jc001256
- Candela, J., Ochoa, J., Sheinbaum, J., López, M., Pérez-Brunius, P., Tenreiro, M.,

  ... Arriaza-Oliveros, L. (2019, June). The flow through the gulf of mexico.

  Journal of Physical Oceanography, 49(6), 1381–1401. Retrieved from http://

  dx.doi.org/10.1175/JPO-D-18-0189.1 doi: 10.1175/jpo-d-18-0189.1
- Candela, J., Sheinbaum, J., Ochoa, J., Badan, A., & Leben, R. (2002, November). The potential vorticity flux through the yucatan channel and the loop current in the gulf of mexico. Geophysical Research Letters, 29(22), 16–1–16–4. Retrieved from https://doi.org/10.1029/2002g1015587 doi: 10.1029/2002g1015587
- Chelton, D. B., Schlax, M. G., & Samelson, R. M. (2011, October). Global observations of nonlinear mesoscale eddies. *Progress in Oceanography*, 91(2), 167–216. Retrieved from http://dx.doi.org/10.1016/j.pocean.2011.01.002 doi: 10 .1016/j.pocean.2011.01.002
- Chérubin, L. M., Morel, Y., & Chassignet, E. P. (2006, April). Loop current ring shedding: The formation of cyclones and the effect of topography. *Journal of Physical Oceanography*, 36(4), 569–591. Retrieved from https://doi.org/10 .1175/jpo2871.1 doi: 10.1175/jpo2871.1
- Cochrane, J. (1972). Separation of an anticyclone and subsequent developments in the loop current (1969). Contributions on the Physical Oceanography of the

```
Gulf of Mexico, 2, 91–106.
505
      Donohue, K., Watts, D., Hamilton, P., Leben, R., Kennelly, M., & Lugo-Fernández,
506
            A. (2016, December). Gulf of mexico loop current path variability. Dynamics
507
            of Atmospheres and Oceans, 76, 174-194. Retrieved from https://doi.org/
508
            10.1016/j.dynatmoce.2015.12.003 doi: 10.1016/j.dynatmoce.2015.12.003
509
      Dukhovskoy, D. S., Leben, R. R., Chassignet, E. P., Hall, C. A., Morey, S. L., &
            Nedbor-Gross, R.
                                (2015, June).
                                                Characterization of the uncertainty of loop
511
            current metrics using a multidecadal numerical simulation and altimeter ob-
512
                           Deep Sea Research Part I: Oceanographic Research Papers, 100,
            servations.
513
            140-158.
                        Retrieved from http://dx.doi.org/10.1016/j.dsr.2015.01.005
514
            doi: 10.1016/j.dsr.2015.01.005
      Durante, G., Candela, J., & Sheinbaum, J. (2023). Canek database v0: Gridded data
516
            from a mooring section across the yucatan channel. Zenodo.
                                                                           Retrieved from
517
            https://zenodo.org/doi/10.5281/zenodo.7865542 doi: 10.5281/ZENODO
518
            .7865542
      Elliott, B. A.
                      (1982, November).
                                          Anticyclonic rings in the gulf of mexico.
520
            nal of Physical Oceanography, 12(11), 1292-1309. Retrieved from https://doi
521
            .org/10.1175/1520-0485(1982)012<1292:aritgo>2.0.co;2
                                                                             doi: 10.1175/
522
            1520-0485(1982)012\langle 1292:aritgo \rangle 2.0.co; 2
523
      European Union-Copernicus Marine Service.
                                                      (2015).
                                                                  Global ocean gridded nor-
524
            malized measurement noise of sea level anomalies.
                                                                    Mercator Ocean Inter-
525
            national.
                             Retrieved from https://resources.marine.copernicus.eu/
526
            product-detail/SEALEVEL_GLO_PHY_NOISE_L4_STATIC_008_033/INFORMATION
            doi: 10.48670/MOI-00144
528
      Fratantoni, P. S., Lee, T. N., Podesta, G. P., & Muller-Karger, F.
                                                                              (1998, Octo-
529
                          The influence of loop current perturbations on the formation and
530
            evolution of tortugas eddies in the southern straits of florida.
                                                                                Journal of
531
            Geophysical Research: Oceans, 103(C11), 24759–24779.
                                                                            Retrieved from
532
            https://doi.org/10.1029/98jc02147 doi: 10.1029/98jc02147
533
      Garcia-Jove, M., Sheinbaum, J., & Jouanno, J.
                                                        (2016, July).
                                                                        Sensitivity of loop
534
            current metrics and eddy detachments to different model configurations: The
535
            impact of topography and caribbean perturbations.
                                                                   Atmósfera, 29(3), 235-
536
                 Retrieved from https://doi.org/10.20937/atm.2016.29.03.05
537
            10.20937/atm.2016.29.03.05
538
      Hamilton, P., Leben, R., Bower, A., Furey, H., & Pérez-Brunius, P.
                                                                             (2018, April).
            Hydrography of the gulf of mexico using autonomous floats.
                                                                                Journal of
540
            Physical Oceanography, 48(4), 773–794.
                                                        Retrieved from https://doi.org/
```

```
10.1175/jpo-d-17-0205.1 doi: 10.1175/jpo-d-17-0205.1
542
      Hamilton, P., Lugo-Fernández, A., & Sheinbaum, J. (2016, December). A loop cur-
543
            rent experiment: Field and remote measurements.
                                                                 Dynamics of Atmospheres
544
            and Oceans, 76, 156-173.
                                            Retrieved from http://dx.doi.org/10.1016/
545
            j.dynatmoce.2016.01.005 doi: 10.1016/j.dynatmoce.2016.01.005
546
      Hiron, L., Cruz, B. J., & Shay, L. K. (2020, March). Evidence of loop current frontal
            eddy intensification through local linear and nonlinear interactions with the
548
            loop current. Journal of Geophysical Research: Oceans, 125(4). Retrieved from
549
            https://doi.org/10.1029/2019jc015533 doi: 10.1029/2019jc015533
550
      Hogg, A. M., Meredith, M. P., Chambers, D. P., Abrahamsen, E. P., Hughes, C. W.,
551
            & Morrison, A. K. (2015, January). Recent trends in the jscp;si/scp;outhern
552
            jscpioj/scpicean eddy field. Journal of Geophysical Research: Oceans, 120(1),
            257-267. Retrieved from http://dx.doi.org/10.1002/2014JC010470
            10.1002/2014jc010470
555
      Hurlburt, H. E., & Thompson, J. D.
                                               (1980, October).
                                                                     A numerical study of
556
                                                              Journal of Physical Oceanog-
            loop current intrusions and eddy shedding.
557
            raphy, 10(10), 1611-1651.
                                              Retrieved from https://doi.org/10.1175/
558
            1520-0485(1980)010<1611:ansolc>2.0.co;2
                                                             doi: 10.1175/1520-0485(1980)
559
            010\langle 1611:ansolc \rangle 2.0.co; 2
      Jouanno, J., Ochoa, J., Pallàs-Sanz, E., Sheinbaum, J., Andrade-Canto, F., Can-
561
            dela, J., & Molines, J.-M.
                                          (2016, November).
                                                                  Loop current frontal ed-
562
            dies: Formation along the campeche bank and impact of coastally trapped
563
            waves. Journal of Physical Oceanography, 46(11), 3339–3363. Retrieved from
            https://doi.org/10.1175/jpo-d-16-0052.1 doi: 10.1175/jpo-d-16-0052.1
565
      Jousset, S., Mulet, S., Greiner, E., et al.
                                                    (2025, February 25).
                                                                               New global
566
            mean dynamic topography cnes-cls-22 combining drifters, hydrography
567
            profiles and high frequency radar data.
                                                        ESS Open Archive.
                                                                                 Retrieved
568
            from https://doi.org/10.22541/essoar.170158328.85804859/v2
                                                                                       doi:
569
            10.22541/essoar.170158328.85804859/v2
570
      Kantha, L.
                      (2014, May).
                                        Empirical models of the loop current eddy detach-
571
            ment/separation time in the gulf of mexico.
                                                               Journal of Waterway, Port,
572
            Coastal, and Ocean Engineering, 140(3).
                                                        Retrieved from https://doi.org/
573
            10.1061/(asce)ww.1943-5460.0000220
                                                          doi: 10.1061/(asce)ww.1943-5460
574
            .0000220
575
      Larrañaga, M., Renault, L., & Jouanno, J.
                                                    (2022).
                                                              Partial control of the gulf of
            mexico dynamics by the current feedback to the atmosphere.
577
            Physical Oceanography.
                                        Retrieved from https://journals.ametsoc.org/
578
```

- view/journals/phoc/aop/JPO-D-21-0271.1/JPO-D-21-0271.1.xml doi: 10.1175/JPO-D-21-0271.1
- Larrañaga, M., Renault, L., Wineteer, A., Contreras, M., Arbic, B. K., Bourassa,

  M. A., & Rodriguez, E. (2025, January). Assessing the future odysea satel
  lite mission for the estimation of ocean surface currents, wind stress, energy

  fluxes, and the mechanical coupling between the ocean and the atmosphere.

  Remote Sensing, 17(2), 302. Retrieved from http://dx.doi.org/10.3390/

  rs17020302 doi: 10.3390/rs17020302
- Laxenaire, R., Chassignet, E. P., Dukhovskoy, D. S., & Morey, S. L. (2023, February). Impact of upstream variability on the loop current dynamics in numerical
  simulations of the gulf of mexico. Frontiers in Marine Science, 10. Retrieved
  from http://dx.doi.org/10.3389/fmars.2023.1080779 doi: 10.3389/fmars
  .2023.1080779
- Le Hénaff, M., Kourafalou, V. H., Morel, Y., & Srinivasan, A. (2012, February).

  Simulating the dynamics and intensification of cyclonic loop current frontal eddies in the gulf of mexico. *Journal of Geophysical Research: Oceans*, 117(C2),

  n/a-n/a. Retrieved from https://doi.org/10.1029/2011jc007279 doi:
  10.1029/2011jc007279
- Leben, R. R. (2005). Altimeter-derived loop current metrics. Geophysical

  Monograph-American Geophysical Union, 161, 181.
- Le Hénaff, M., Kourafalou, V. H., Androulidakis, Y., Ntaganou, N., & Kang, H.

  (2023). Influence of the caribbean sea eddy field on loop current predictions.

  Frontiers in Marine Science.
- Lugo-Fernández, A., & Leben, R. R. (2010, December). On the linear relationship between loop current retreat latitude and eddy separation period. *Journal*of Physical Oceanography, 40(12), 2778–2784. Retrieved from http://dx.doi
  .org/10.1175/2010JP04354.1 doi: 10.1175/2010jpo4354.1
- Meunier, T., Pallás-Sanz, E., Tenreiro, M., Portela, E., Ochoa, J., Ruiz-Angulo, A.,

  & Cusí, S. (2018, September). The vertical structure of a loop current eddy.

  Journal of Geophysical Research: Oceans, 123(9), 6070–6090. Retrieved from

  https://doi.org/10.1029/2018jc013801 doi: 10.1029/2018jc013801
- Meunier, T., Sheinbaum, J., Pallàs-Sanz, E., Tenreiro, M., Ochoa, J., Ruiz-Angulo,
  A., ... de Marez, C. (2020, February). Heat content anomaly and decay of
  warm-core rings: the case of the gulf of mexico. Geophysical Research Letters, 47(3). Retrieved from https://doi.org/10.1029/2019g1085600 doi:
  10.1029/2019g1085600
  - Molina, M. J., Timmer, R. P., & Allen, J. T. (2016, December). Importance of the

- gulf of mexico as a climate driver for u.s. severe thunderstorm activity. Geo-616 physical Research Letters, 43(23). Retrieved from https://doi.org/10.1002/ 617 2016g1071603 doi: 10.1002/2016gl071603 Morrow, R., Fu, L.-L., Ardhuin, F., Benkiran, M., Chapron, B., Cosme, E., ... 619 Zaron, E. D. (2019). Global observations of fine-scale ocean surface topography with the surface water and ocean topography (swot) mission. Frontiers in 621 Marine Science, 6, 1–19. Nickerson, A. K., Weisberg, R. H., & Liu, Y. (2022, June). On the evolution of 623 the gulf of mexico loop current through its penetrative, ring shedding and 624 Advances in Space Research, 69(11), 4058–4077. Reretracted states. 625 trieved from http://dx.doi.org/10.1016/j.asr.2022.03.039 doi: 10.1016/j.asr.2022.03.039 627 Pegliasco, C., Delepoulle, A., Mason, E., Morrow, R., Faugère, Y., & Dibarboure, 628 (2022, March). Meta3.1exp: a new global mesoscale eddy trajectory at-629 las derived from altimetry. Earth System Science Data, 14(3), 1087–1107. Retrieved from http://dx.doi.org/10.5194/essd-14-1087-2022 doi: 631
- 10.5194/essd-14-1087-2022632
- Pichevin, T., & Nof, D. (1997, March). The momentum imbalance paradox. Tellus 633 Retrieved from https://doi.org/10.1034/j.1600-0870 A, 49(2), 298-319.634 .1997.t01-1-00009.x doi: 10.1034/j.1600-0870.1997.t01-1-00009.x 635
- Rodríguez, E., Bourassa, M., Chelton, D., Farrar, J. T., Long, D., Perkovic-Martin, D., & Samelson, R. (2019, July). The winds and currents mission concept. 637 Retrieved from https://doi.org/10.3389/ Frontiers in Marine Science, 6. 638 fmars.2019.00438 doi: 10.3389/fmars.2019.00438 639
- Schmitz, W. J. (2005, March). Cyclones and westward propagation in the shed-640 ding of anticyclonic rings from the loop current. In Circulation in the gulf of 641 mexico: Observations and models (pp. 241–261). American Geophysical Union. 642 doi: 10.1029/161gm18 643
- Sheinbaum, J. (2002). Flow structure and transport in the yucatan channel. Geophysical Research Letters, 29(3). Retrieved from https://doi.org/10.1029/ 645 2001g1013990 doi: 10.1029/2001gl013990 646
- Sheinbaum, J., Athié, G., Candela, J., Ochoa, J., & Romero-Arteaga, A. (2016, De-647 cember). Structure and variability of the yucatan and loop currents along the slope and shelf break of the yucatan channel and campeche bank. Dynamics of 649 Atmospheres and Oceans, 76, 217–239. Retrieved from https://doi.org/10 650 .1016/j.dynatmoce.2016.08.001 doi: 10.1016/j.dynatmoce.2016.08.001 651
- Sosa-Gutiérrez, R., Pallàs-Sanz, E., Jouanno, J., Chaigneau, A., Candela, J., & Ten-652

```
reiro, M. (2020). Erosion of the subsurface salinity maximum of the loop
current eddies from glider observations and a numerical model. Journal of
Geophysical Research: Oceans, 125(7), e2019JC015397.
```

- Torres, H., Wineteer, A., Klein, P., Lee, T., Wang, J., Rodriguez, E., ... Zhang, H.

  (2023, June). Anticipated capabilities of the odysea wind and current mission concept to estimate wind work at the air-sea interface. Remote Sensing,

  15(13), 3337. Retrieved from http://dx.doi.org/10.3390/rs15133337 doi:
  10.3390/rs151333337
- Vukovich, F. M., & Maul, G. A. (1985, January). Cyclonic eddies in the eastern gulf
  of mexico. Journal of Physical Oceanography, 15(1), 105–117. Retrieved from
  https://doi.org/10.1175/1520-0485(1985)015<0105:ceiteg>2.0.co;2
  doi: 10.1175/1520-0485(1985)015\(0105:ceiteg\)2.0.co;2
- Wineteer, A., Torres, H. S., & Rodriguez, E. (2020, October). On the surface current measurement capabilities of spaceborne doppler scatterometry. Geophysical Research Letters, 47(21). Retrieved from http://dx.doi.org/10.1029/2020GL090116 doi: 10.1029/2020gl090116
- Yablonsky, R. M., & Ginis, I. (2012, March). Impact of a warm ocean eddy's circulation on hurricane-induced sea surface cooling with implications for hurricane intensity. *Monthly Weather Review*, 141(3), 997–1021.

  Retrieved from https://doi.org/10.1175/mwr-d-12-00248.1 doi: 10.1175/mwr-d-12-00248.1
- Yang, H., Yang, C., Liu, Y., & Chen, Z. (2023, February). Energetics during eddy shedding in the gulf of mexico. Ocean Dynamics, 73(2), 79–90. Retrieved from http://dx.doi.org/10.1007/s10236-023-01538-y doi: 10.1007/s10236-023-01538-y
- Zavala-Hidalgo, J., Morey, S., O'brien, J., & Zamudio, L. (2006). On the loop current eddy shedding variability. *Atmósfera*, 19(1), 41–48.
- Zavala-Hidalgo, J., Morey, S. L., & O'Brien, J. J. (2003, March). Cyclonic eddies northeast of the campeche bank from altimetry data. *Journal of Physical Oceanography*, 33(3), 623–629. Retrieved from https://doi.org/10.1175/1520-0485(2003)033<0623:cenotc>2.0.co;2 doi: 10.1175/1520-0485(2003)033\delta(0623:cenotc\delta(2.0.co;2)

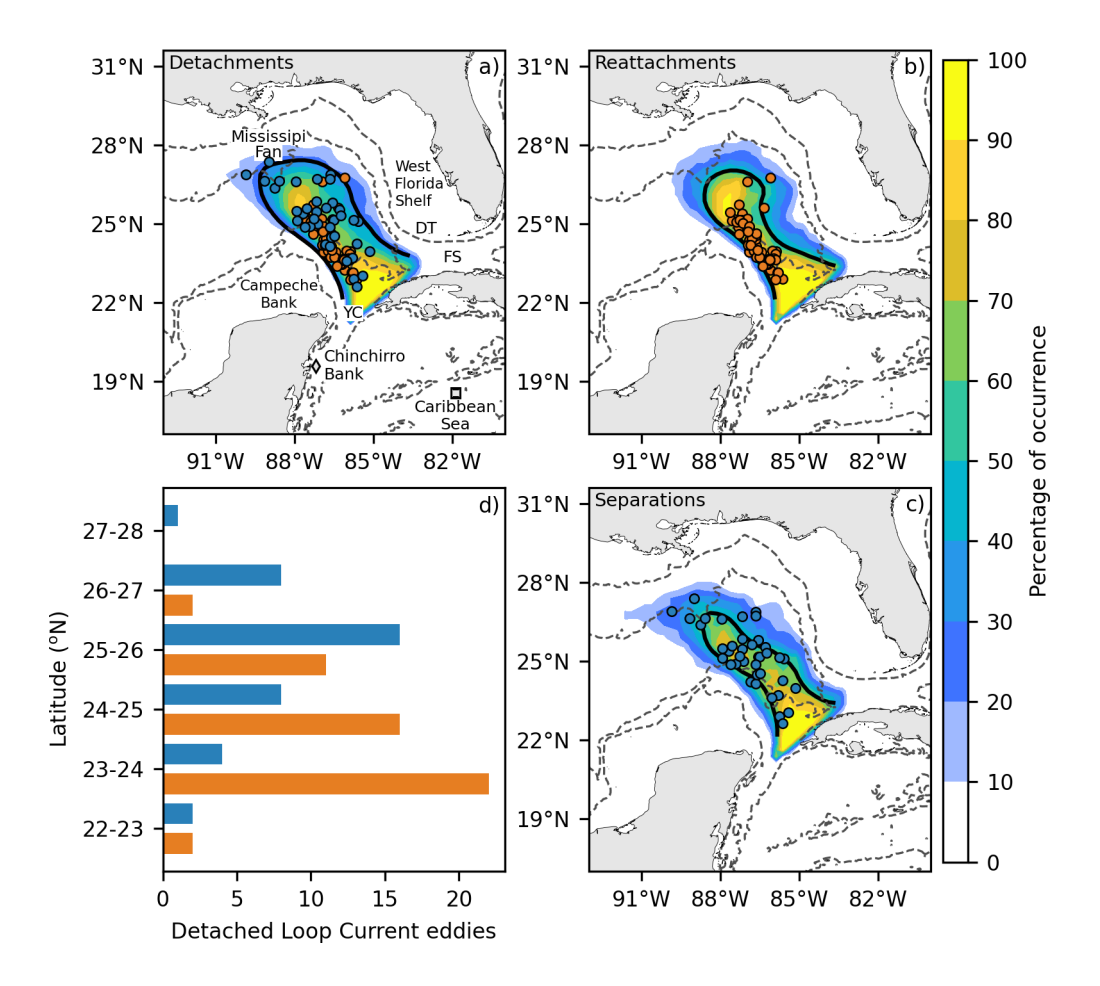


Figure 1. a) detachment locations (a), leading to reattachment (b) and separation (c) events (orange/blue circles, respectively). A probability density function of the LC spatial occurrence one day before the LCEs detachment is depicted by the shaded area. The averaged position of the LC one day before the detachment of LCEs is represented by the black contour. d) Histogram related to the number of reattachments (orange) and separations (blue) as a function of their latitude of occurrence. YCH refers to the Yucatan Channel, FS to the Florida Straits, DT to the Dry Tortugas, and MF to the Mississippi Fan. The light gray contours refer to the 200 m (continuous) and 2500 m (dashed) depths. The gray square in the Caribbean Sea represents the starting point for the transects utilized to generate the Hovmöller diagrams shown in Figure 11, whereas the gray diamond represents the location of the Chinchorro Bank.

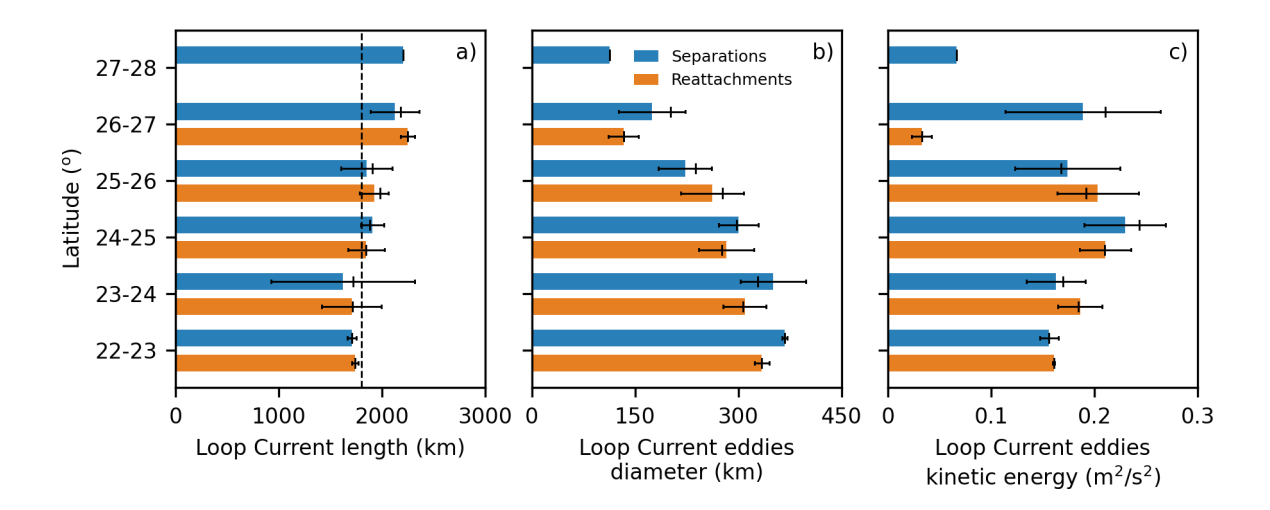


Figure 2. Statistics about the LC length one day before a LCE detachment (a), as well as the diameter (b) and kinetic energy (c) of detached LCEs are presented for the different regions. The statistics are calculated across all cases within each latitudinal category. Separations are depicted with blue bars, whereas reattachments are depicted with orange bars. The standard deviation is represented by error bars, while the longer vertical lines indicate the median. The segmented black line in a) represents the 1800 km LC length threshold.

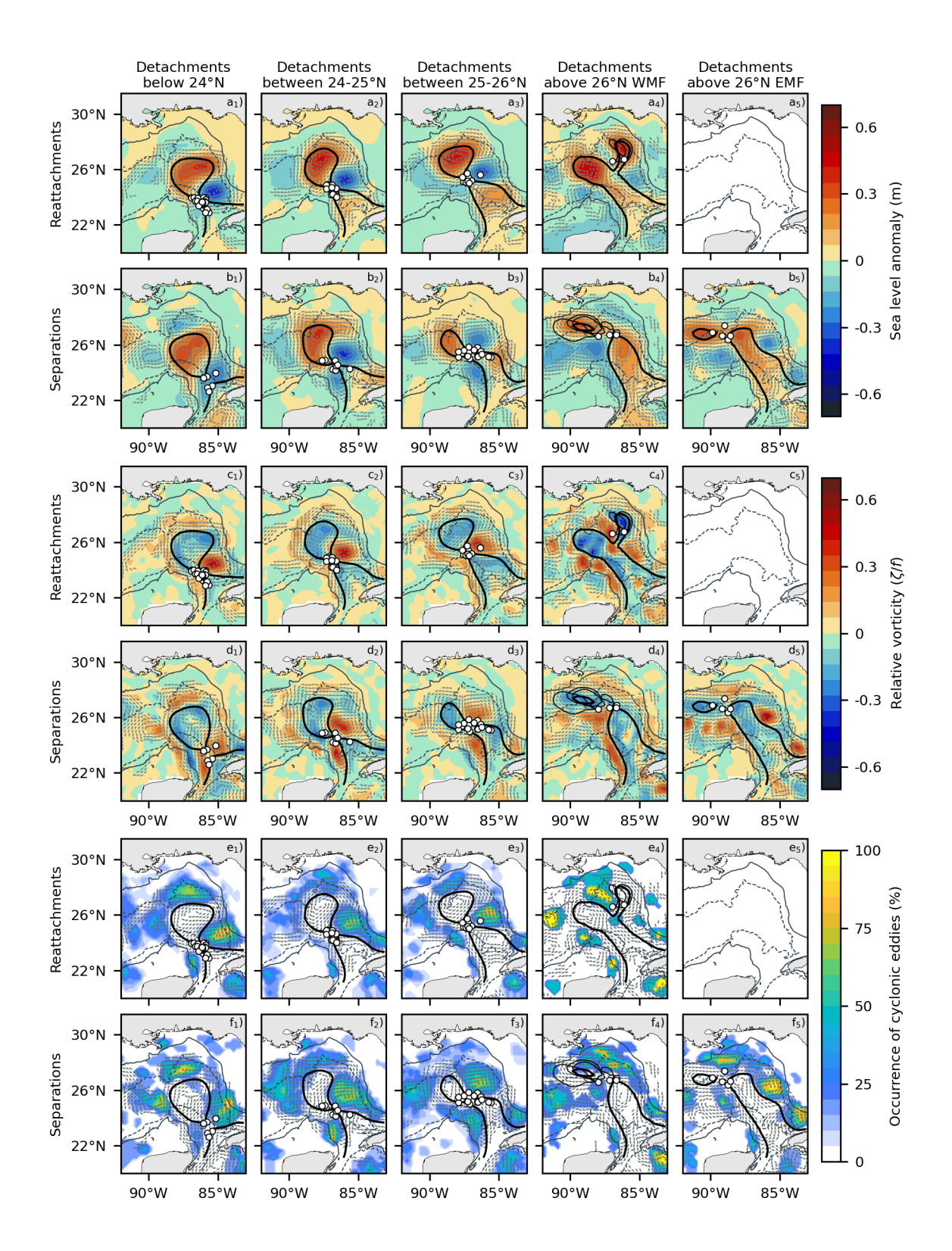
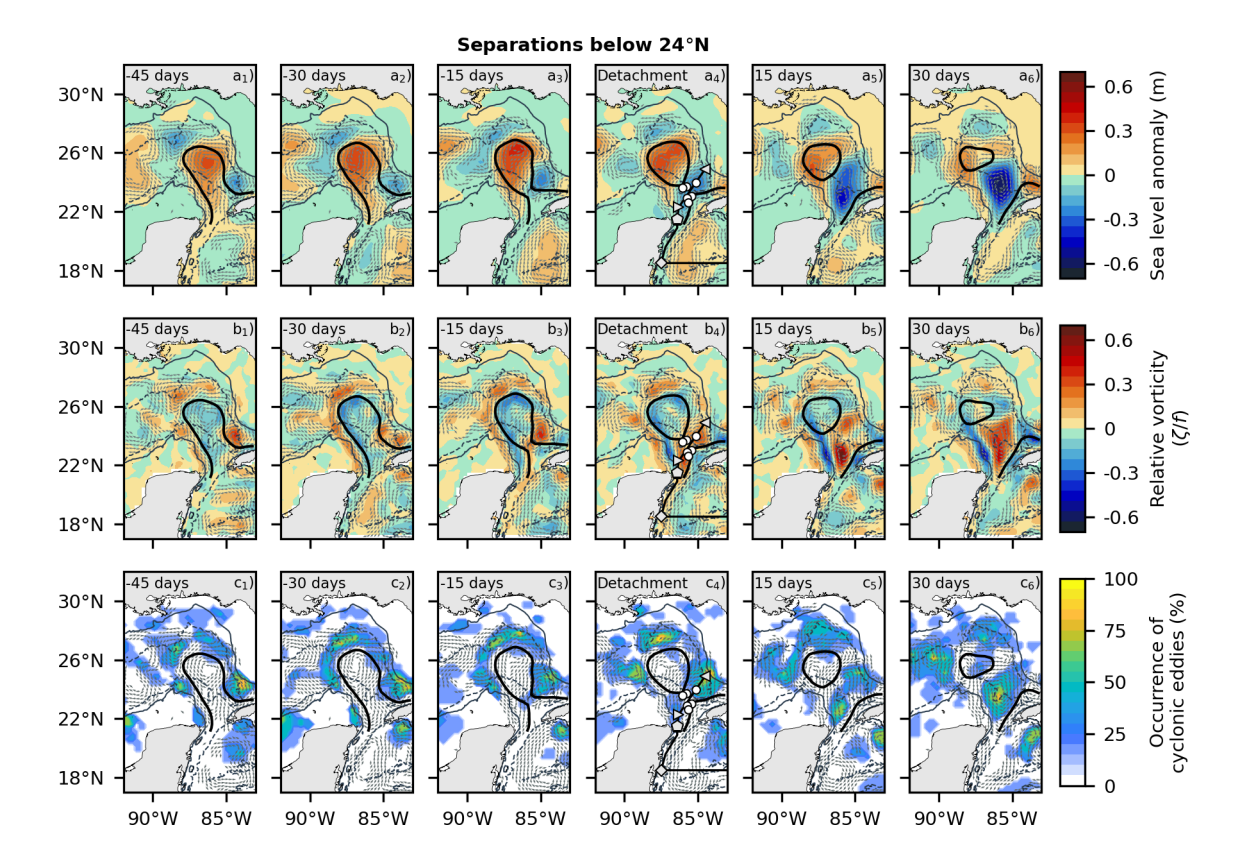
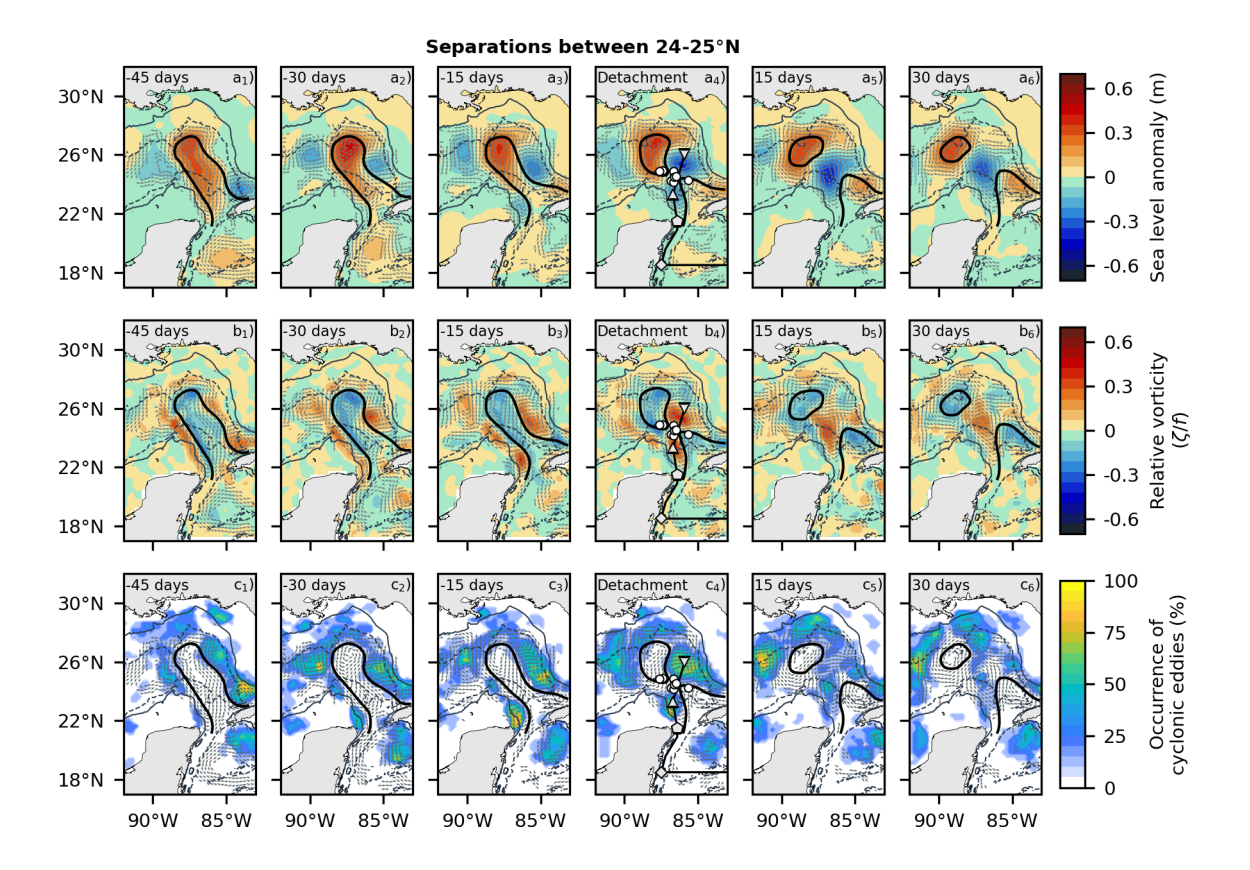


Figure 3. SLA composites during LCEs detachment that ends in reattachments (first row) and separation (second row) for the different LC regions with eddy shedding (different columns). Thick contours represent the composite LC and detached LCEs. Relative vorticity composites are depicted in the third (reattachments) and fourth (separations) rows. The histograms of the occurrence of cyclonic eddies during detachments leading to reattachments and separations are depicted in the fifth and sixth rows, respectively. Thin contours in the last column represent the LCEs for each detachment case in the region. The gray arrows depict the direction of surface geostrophic currents with speeds stronger than 0.1 m s<sup>-1</sup>. White circles represent the LC outer-



**Figure 4.** Time evolution of SLA (first row) and Rossby number (second row) composites, as well as the probability of cyclonic eddies occurrence (third row) during LCEs separation below 24°N. Thick contours represent the composite LC and detached LCEs. Thin contours in the last three represent the LCEs for each detachment case in the region. The gray arrows depict the direction of surface geostrophic currents with speeds stronger than 0.1 m s<sup>-1</sup>. White circles represent the LC outermost position after detachment events used for the composites. The light gray contours refer to the 200 m (continuous) and 2500 m (dashed) depths.



**Figure 5.** Time evolution of SLA (first row) and Rossby number (second row) composites, as well as the probability of cyclonic eddies occurrence (third row) during LCEs separation between 24 and 25°N. Thick contours represent the composite LC and detached LCEs. Thin contours in the last three represent the LCEs for each detachment case in the region. The gray arrows depict the direction of surface geostrophic currents with speeds stronger than 0.1 m s<sup>-1</sup>. White circles represent the LC outermost position after detachment events used for the composites. The light gray contours refer to the 200 m (continuous) and 2500 m (dashed) depths.

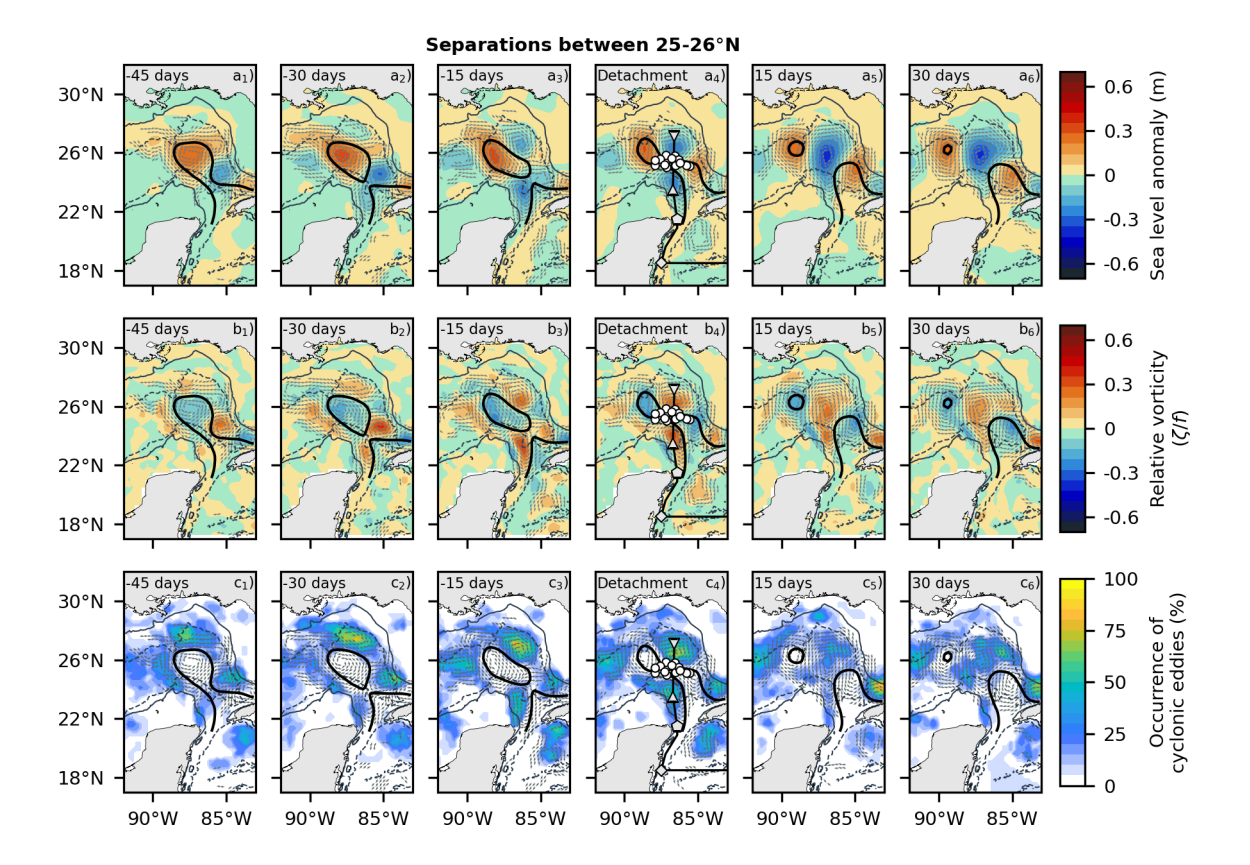


**Figure 6.** Time evolution of SLA (first row) and Rossby number (second row) composites, as well as the probability of cyclonic eddies occurrence (third row) during LCEs separation between 25 and 26°N. Thick contours represent the composite LC and detached LCEs. Thin contours in the last three represent the LCEs for each detachment case in the region. The gray arrows depict the direction of surface geostrophic currents with speeds stronger than 0.1 m s<sup>-1</sup>. White circles represent the LC outermost position after detachment events used for the composites. The light gray contours refer to the 200 m (continuous) and 2500 m (dashed) depths.

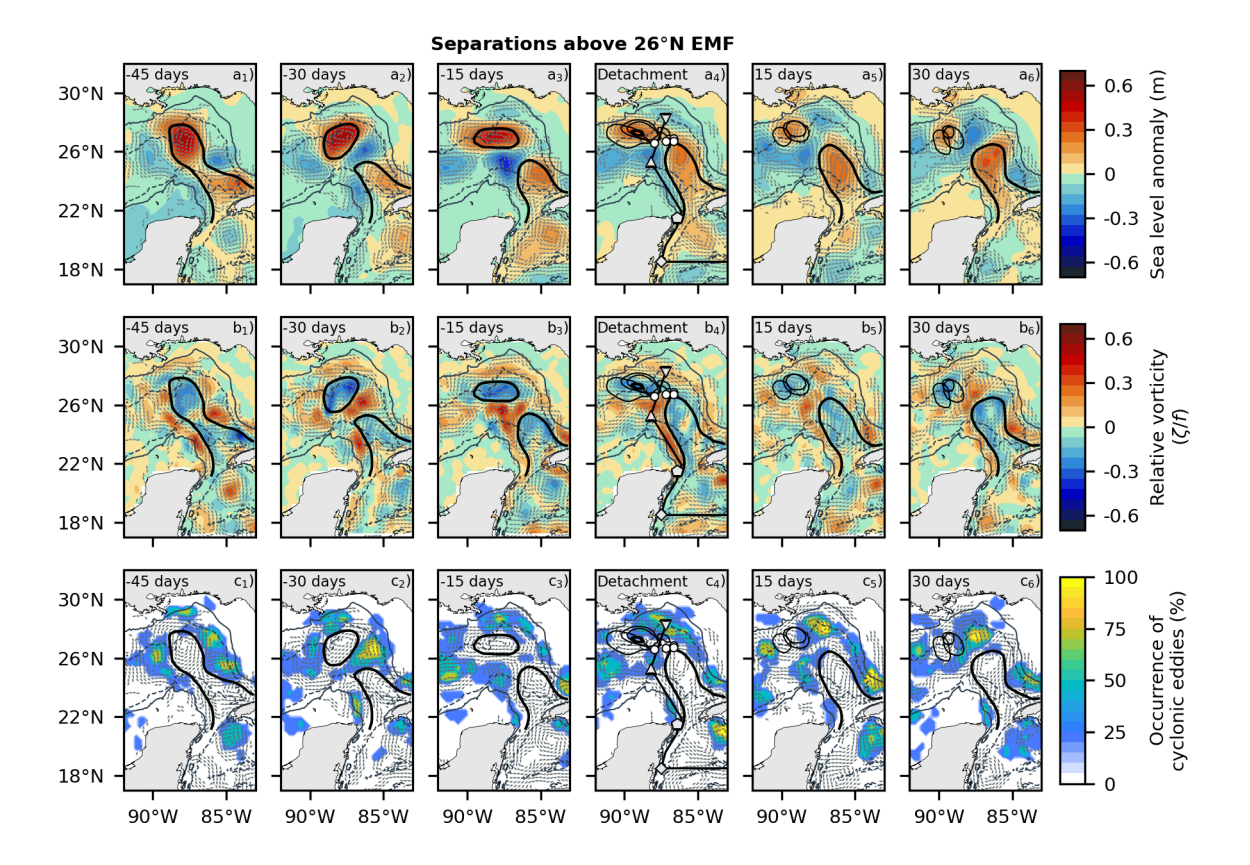


Figure 7. Time evolution of SLA (first row) and Rossby number (second row) composites, as well as the probability of cyclonic eddies occurrence (third row) during LCEs separation above 26°N east of the Mississippi Fan (EMF). Thick contours represent the composite LC and detached LCEs. Thin contours in the last three represent the LCEs for each detachment case in the region. The gray arrows depict the direction of surface geostrophic currents with speeds stronger than 0.1 m s<sup>-1</sup>. White circles represent the LC outermost position after detachment events used for the composites. The light gray contours refer to the 200 m (continuous) and 2500 m (dashed) depths.

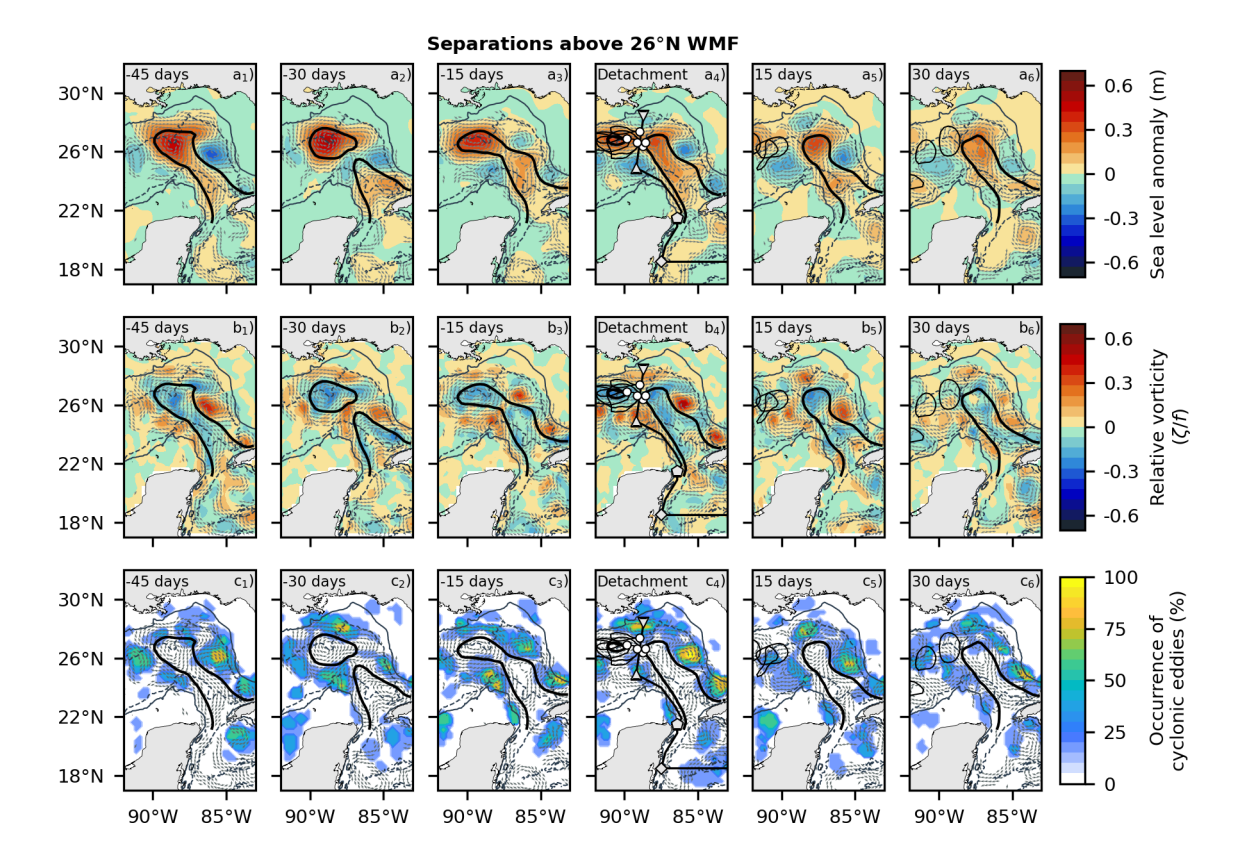
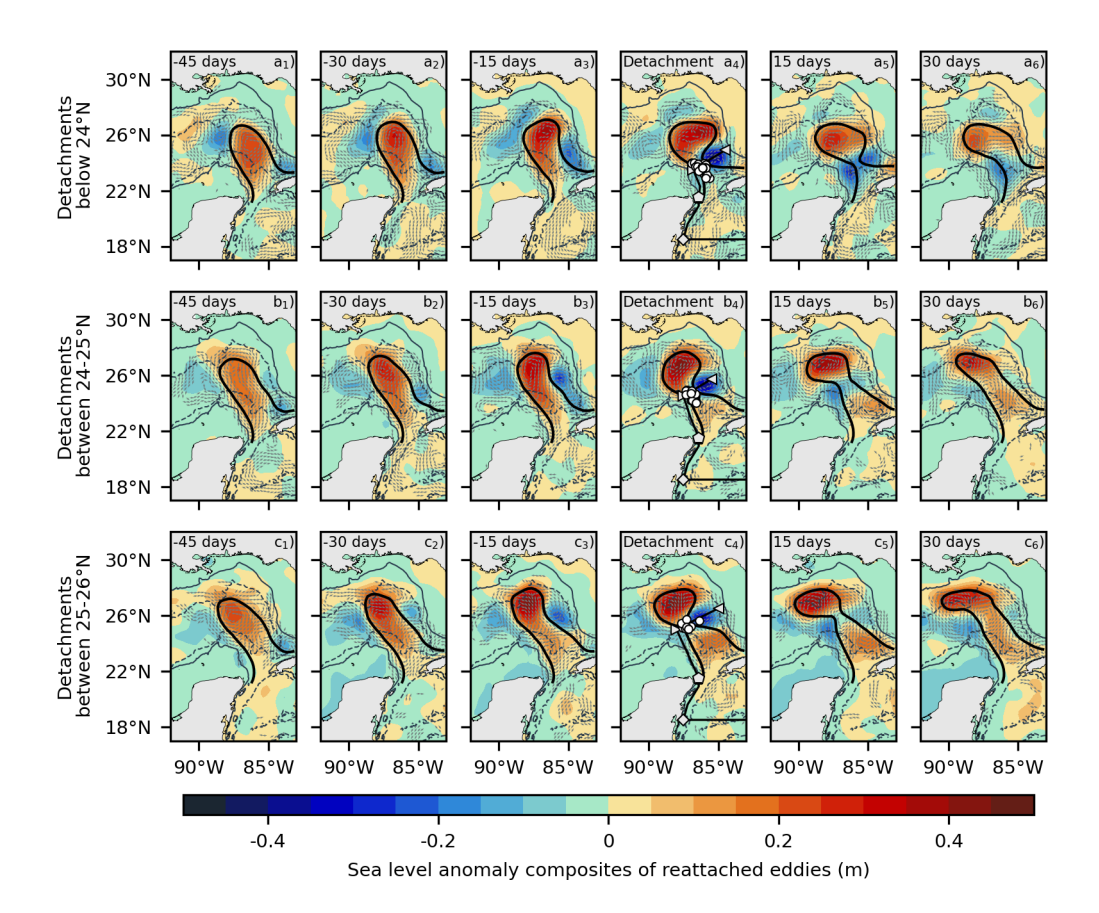


Figure 8. Time evolution of SLA (first row) and Rossby number (second row) composites, as well as the probability of cyclonic eddies occurrence (third row) during LCEs separation above 26°N west of the Mississippi Fan (WMF). Thick contours represent the composite LC and detached LCEs. Thin contours in the last three represent the LCEs for each detachment case in the region. The gray arrows depict the direction of surface geostrophic currents with speeds stronger than 0.1 m s<sup>-1</sup>. White circles represent the LC outermost position after detachment events used for the composites. The light gray contours refer to the 200 m (continuous) and 2500 m (dashed) depths.



**Figure 9.** SLA composites related to detachments occurring below 24°N (first row), between 24 and 25°N, and between 25 and 26°N, that turn into reattachment events. Continued tick black contours represent the LC composite (ADT 17 cm). White circles in the fourth column represent the LC outermost position after detachment events used for the composites. The gray arrows depict the direction of surface geostrophic currents with speeds stronger than 0.1 m s<sup>-1</sup>. The light gray contours refer to the 200 m (continuous) and 2500 m (dashed) depths.

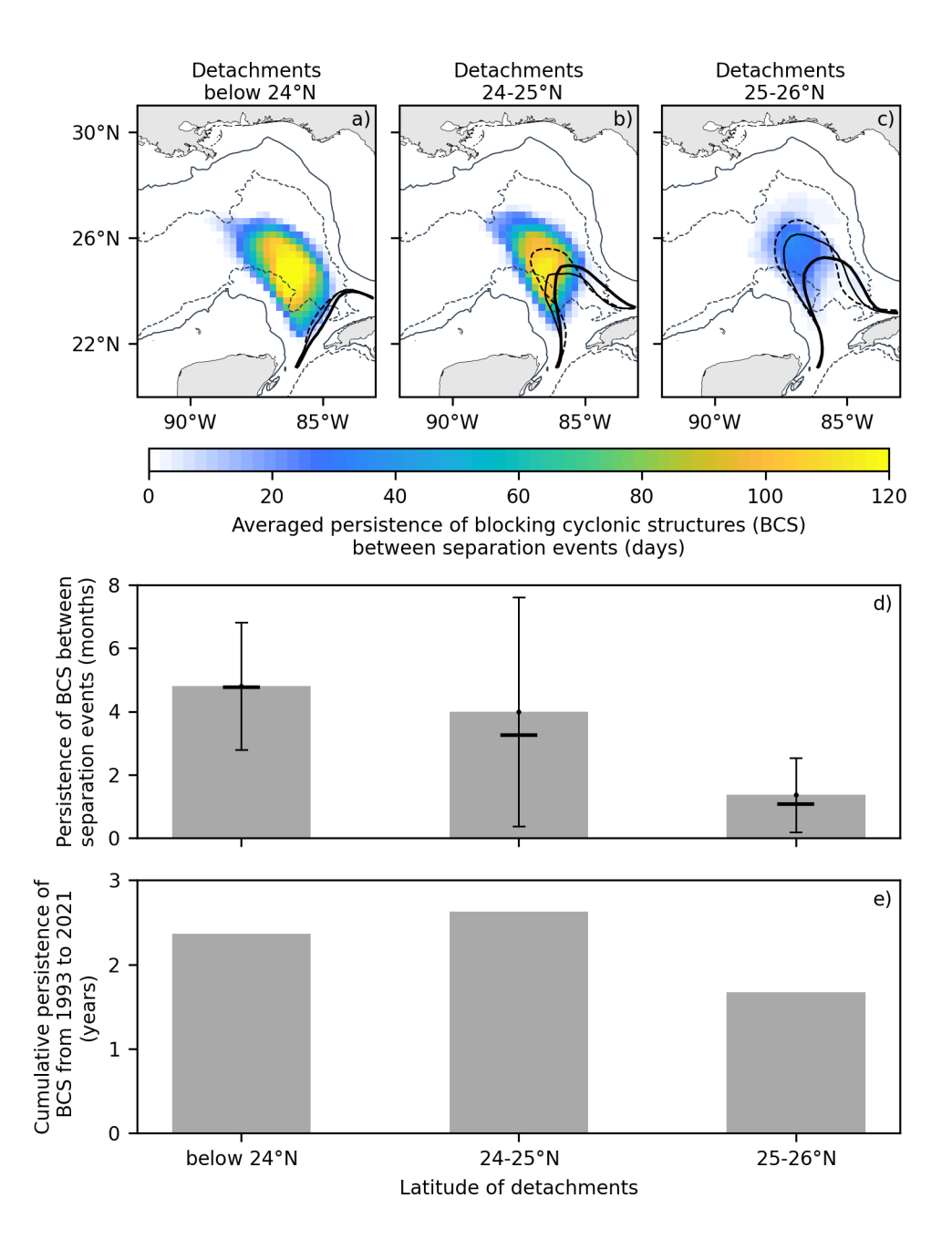


Figure 10. Averaged persistence of blocking cyclonic structures between separation events occurring below 24°N, between 24-26°N, and between 24-26°N. Black contours show the composite LC contour corresponding to 30 days after the detachment of LCEs. The mean, median, and standard deviation of the persistence of blocking cyclonic structures for each region are shown in d. The cumulative persistence of blocking cyclonic structures over the 29-year period is shown in e. The cumulative persistence is computed by multiplying the mean persistence of blocking cyclonic structures by the number of separations per region.

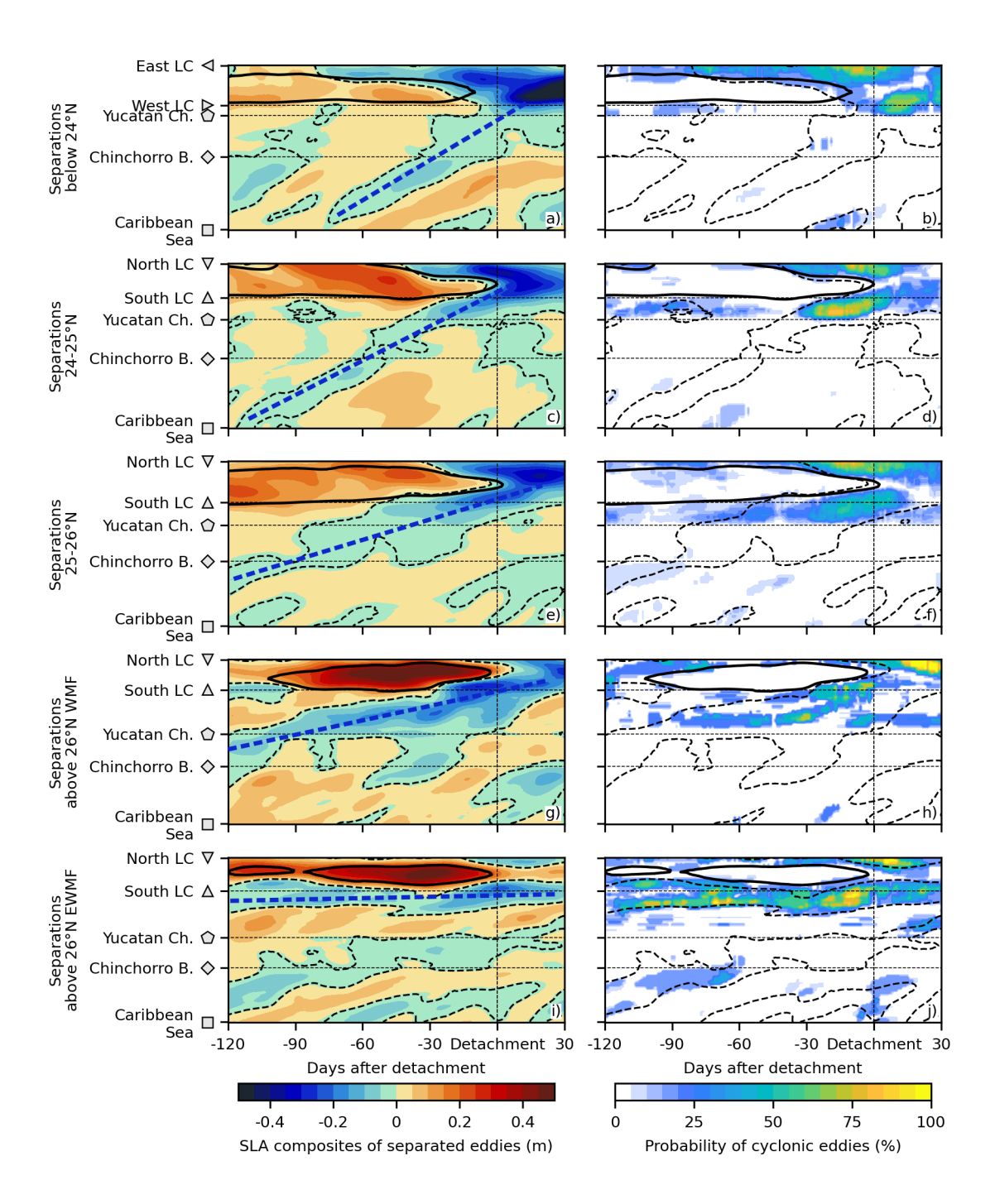


Figure 11. Hovmöller composites of SLA during separations (first column) and the occurrence of cyclonic eddies from the AVISO Atlas (second column) occurring below 24°N (first row), between 24-25°N (second column), between 25-26°N (third column), above 26°N and west of the Mississippi Fan (WMF) (fourth column), and above 26°N and east of the Mississippi Fan (EMF) (fifth column). Thick continuous-black contours represent the composite LC (ADT 17-cm). Thick segmented-black contours depict cyclonic anomalies. Thick segmented-blue contours depict the SLAs propagating from the Caribbean Sea to the GoM. Thin vertical segmented lines exhibit the detachment of LCEs. Horizontal segmented lines indicate the location of the Chinchorro Bank, Yucatan Channel, and the southern region of the LC (western region of the LC in a)).

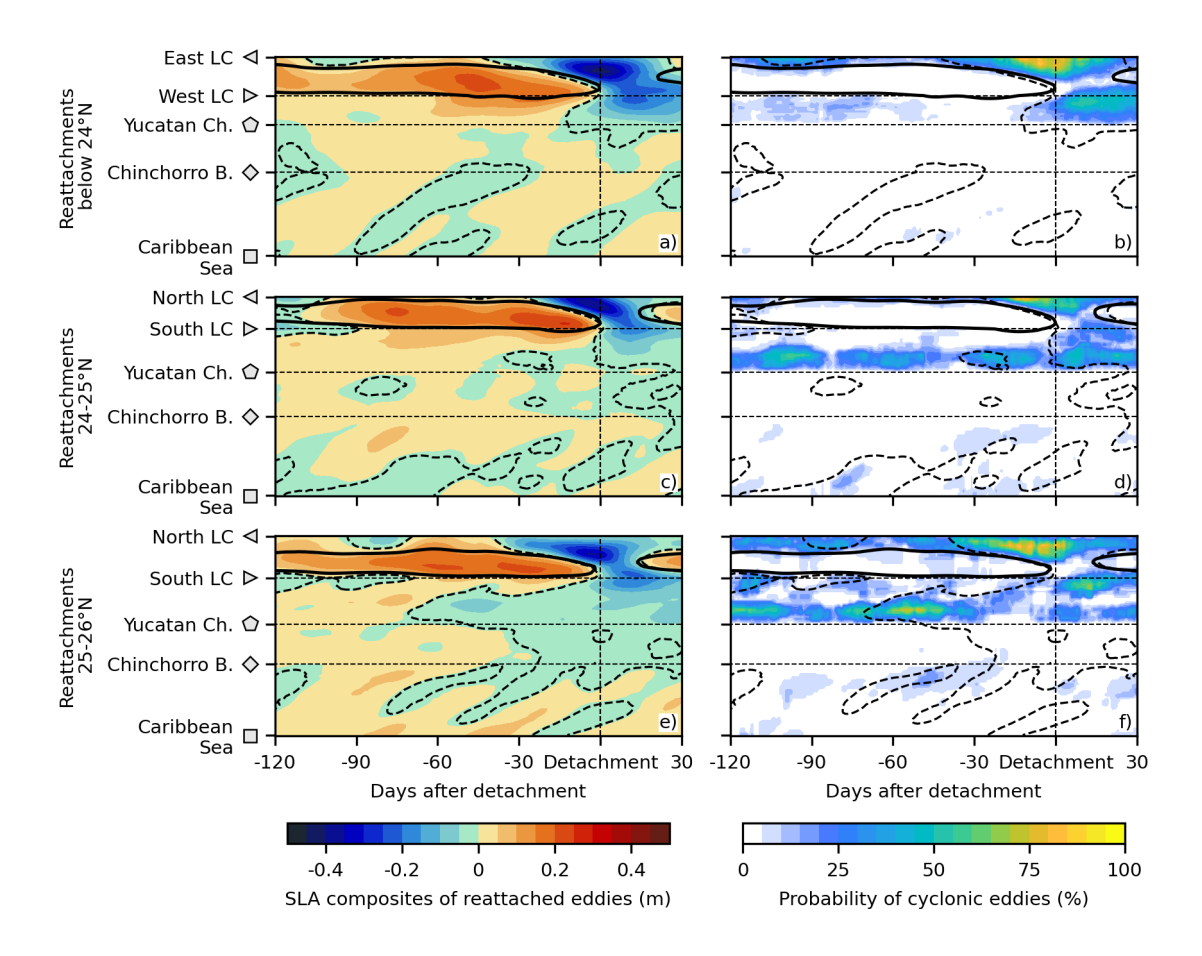


Figure 12. Hovmöller composites of SLA during separations (first column) and the occurrence of cyclonic eddies from the AVISO Atlas (second column) occurring below 24°N (first row), between 24-25°N (second column), between 25-26°N (third column), above 26°N and west of the Mississippi Fan (WMF) (fourth column), and above 26°N and east of the Mississippi Fan (EMF) (fifth column). Thick continuous-black contours represent the composite LC (ADT 17-cm). Thick segmented-black contours depict cyclonic anomalies. Thin vertical segmented lines exhibit the detachment of LCEs. Horizontal segmented lines indicate the location of the Chinchorro Bank, Yucatan Channel, and the southern region of the LC (western region of the LC in a)).

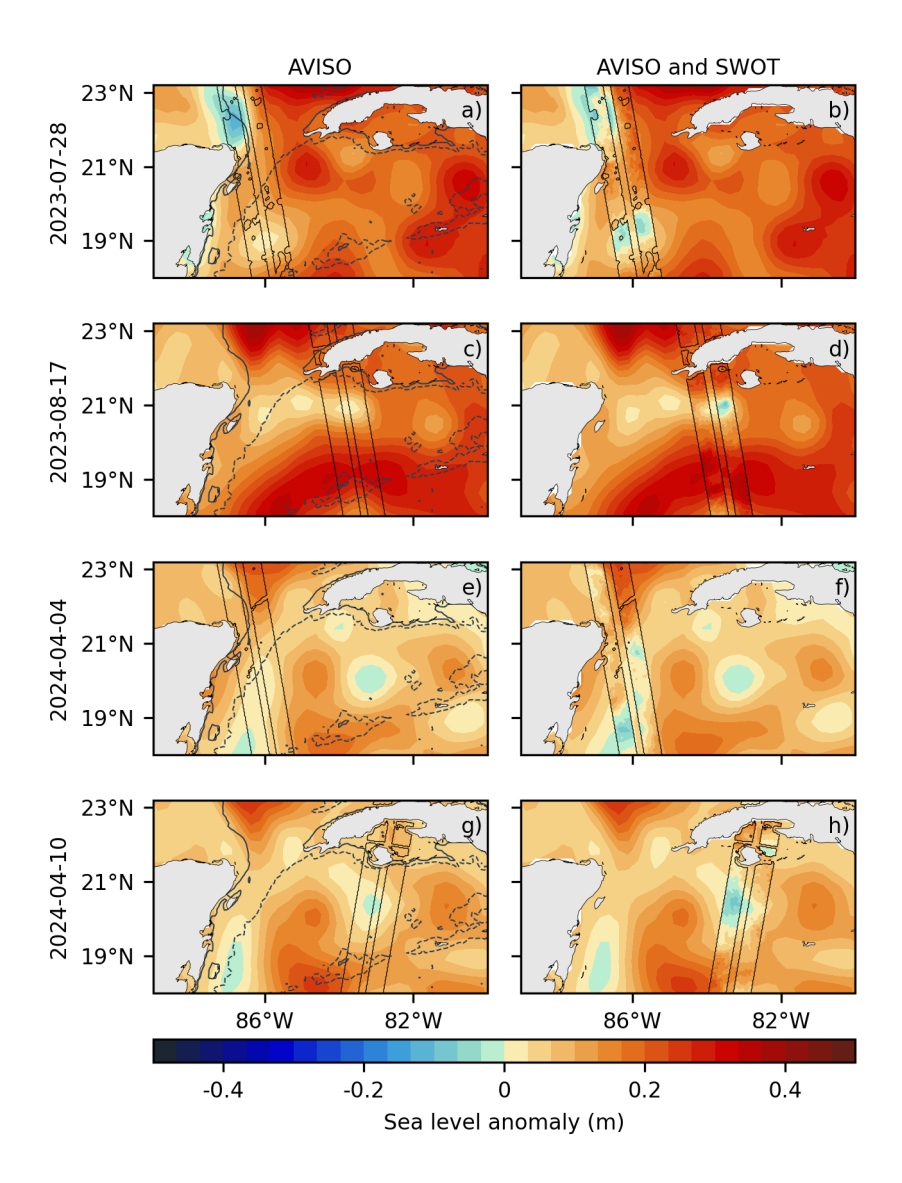
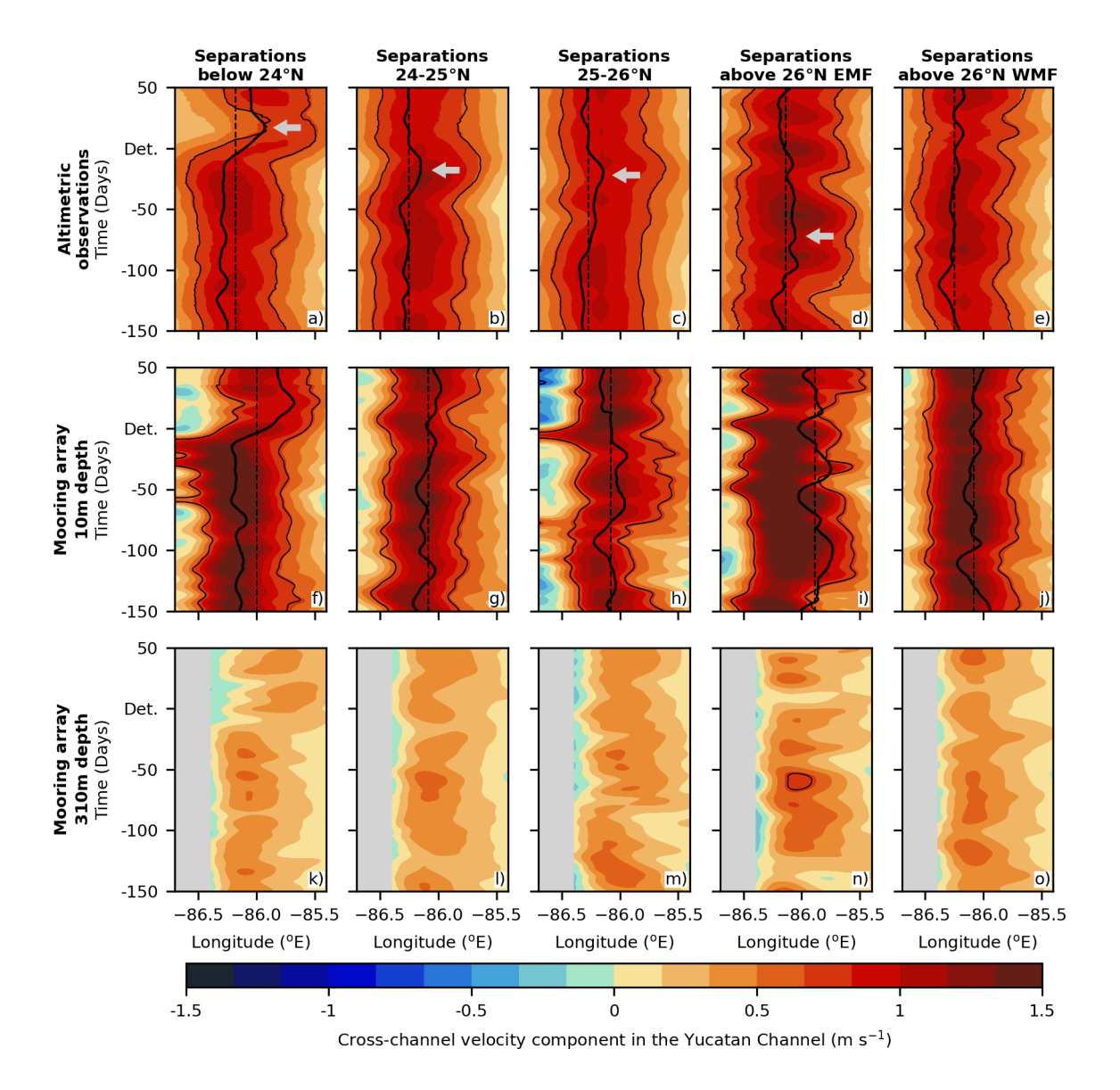


Figure 13. Examples of a comparison between SLA estimations between altimetric gridded maps from CMEMS (first column) and along-track observations from SWOT (second column). Each row refers to a different date. Continuous black contours show the 200-m depth contour, whereas dashed black contours show the 2500-m depth contour. The following describes the differences between the two products. First row: Cyclonic structure around 87°W, 19°N that is not visible in AVISO but is visible in SWOT. Second row: Cyclonic structure around 84°W, 21°N that is not visible in AVISO but is visible in SWOT. Third row: Cyclonic structure around 87°W, 19°N that is not visible in AVISO but is visible in SWOT. Fourth row: Cyclonic structure around 83°W, 21°N that is not visible in AVISO but is visible in SWOT.



Hovmöller composites of the cross-channel current velocity component in the Yucatan Channel from CMEMS (first row) and the CANEK mooring array (10 m depth in the second row and 310 m depth in the third row) during separation events. The columns correspond to separation events occurring below 24°N (first row), between 24-25°N (second column), between 25-26°N (third column), above 26°N and east of the Mississippi Fan (EMF) (fourth column), and above 26°N and east of the Mississippi Fan (EMF) (fifth column). Positive values (red) show northward velocities, whereas negative values (blue) show southward velocities. Thin black curves correspond to the  $0.25 \text{ m}^2 \text{ s}^{-2}$  kinetic energy contour corresponding to the crosschannel current velocity, which is an arbitrary value that helps us to represent the composite LC. Thick black curves correspond to the 17 cm ADT contour from altimetric observations, often used to identify the LC. The thin black segmented line corresponds to the longitude resulting from the time-averaged 17 cm ADT contour between 150 days before and 150 days after the detachment. Gray arrows depict the occurrence 34-eastward displacements of the LC. The number of separation events considered to construct the composites from the mooring array data in the south region corresponds to 2, in the center region to 3, in the north region to 2, in the east upper north region to 1, and in the west upper north region to 2.